Spatial variability of the surface energy balance of Lake Kasumigaura and implications for flux measurements

doi: 10.1080/02626667.2019.1701676

Spatial Variability of the Surface Energy Balance of Lake Kasumigaura and Implications for Flux Measurements

Michiaki Sugita[1]

Hydrological Sciences Journal

https://doi.org/10.1080/02626667.2019.1701676

[1] Faculty of Life and Environmental Sciences, University of Tsukuba, Tsukuba, Ibaraki, Japan

Correspondence to: Michiaki Sugita, Faculty of Life & Environmental Sciences, University of Tsukuba, Tsukuba, Ibaraki 305-8572, Japan. E-mail: sugita@geoenv.tsukuba.ac.jp

Abstract

Spatial variability of lake surface energy balance and its causes are not understood well. 90-m resolution energy balance maps of Lake Kasumigaura (172 km^2) in Japan obtained by interpolating stations' data and bulk equations allowed investigation of these issues. Due to lake-scale variation in meteorological variables and small-scale fluctuations of surface temperature T_s, surface heat fluxes were found differed horizontally at two distinctive scales while radiative fluxes were more uniform. The key variable T_s to surface fluxes was only homogenous for directions with a longer fetch or under calm wind conditions. Using these findings, the suitability of flux station locations, one at the center of the lake and another within a cove, were considered. Although both locations satisfied the fetch requirements, T_s was not always found to be homogeneous in the cove, making this location less suitable for flux measurements, an issue that has been overlooked in scientific communities.

Keywords lake; energy balance; surface temperature; satellite remote sensing; homogeneity; bulk methods

1 INTRODUCTION

1.1 Importance of lakes and water and energy balance studies

Lakes play an important role in local and regional communities. For example, lakes serve as vital water resources, popular tourist destinations (e.g., Kawamura and Fukushima 2018), and are home for organisms such as macrofauna, vegetation, and microbes (e.g., Hoverman and Johnson 2012). Lakes also influence regional climate (e.g., Sills et al. 2011) and the carbon cycle (e.g., Cole et al. 2007). As such, understanding lake water and energy balances that provide basic information regarding the storage and flow of water and energy is important in ascertaining the role of lakes in local to regional scale communities.

Indeed, water balance estimates give information on the amount of water available for daily use as well as water stored in a lake. Change of water storage is a major concern for various organisms living within a lake; it also provides vital information to mitigate possible floods or droughts. Also important for ecosystems and lake water quality is how much water comes from which sources, and how much water discharges to which destinations since the water flow is accompanied usually by the transportation of sediment, nutrients as well as much chemical and biological materials (e.g., Kennedy and Walker 1990, Hemond and Fechner-Levy 2000). Likewise, the energy balance of a lake's surface, the main focus of the present study, gives clear idea on how much energy is consumed in what forms and thus is quite useful to diagnose current state of lake ecosystems. It can be expressed by:

$$R_n = G + L_e E + H \qquad (1)$$

(e.g., Stull, 1988) where R_n is net radiation (W/m^2), G is the net heat flux (W/m^2) through the water's surface into the lake that results in a heat storage change in lake water, L_eE is the latent heat flux (W/m^2) (equal to $L_e \times E$ where L_e is the latent heat of vaporization (J/kg) and E is evaporation (kg /m^2/s), and H is the sensible heat flux (W/m^2).

The importance of energy balance in ecosystems can be understood by noting a few examples. Energy exchange between lake water and the atmosphere determines G, and it is this energy that determines the energy storage and water temperature within a lake. Lake water temperature is a dominant regulator of nearly all physiochemical

cycles and thus lake metabolism and productivity (e.g., Wetzel, 1983, Huang et al. 2019) and lake water quality (e.g., Yang et al. 2018). Energy balance also gives an idea on how much influence a lake exerts on regional climate through its surface energy fluxes (e.g., Notaro et al. 2013) and on a hydrological cycle through the common component of evaporation (Sugita et al. 2014).

1.2 Spatial variability of surface fluxes

In equation (1), the turbulent fluxes L_eE and H are often more difficult to determine than radiative flux R_n. Among available methods, eddy correlation method is preferred because of its higher time resolution and the accuracy of resulting fluxes (e.g., Foken 2008) as compared to other methods such as profile method, Bowen-ratio method, or variance method. Indeed, the eddy correlation method has been applied for lake flux measurements (e.g., Heikinheimo et al. 1999, Blanken et al. 2003, Tanny et al. 2008, Rouse et al. 2008, Nordo et al. 2011, Li et al. 2015). In those studies, fluxes were measured often at a single location within a lake and it was assumed that the measured fluxes represent the whole lake surface or midlake (open water) surface. However, there is no guarantee that this assumption is valid. In fact, it has been reported that there is considerable spatial variability of lake surface properties. Table 1 lists some of the findings of such studies. The target(s), spatial coverage, and time and space resolutions vary a lot in these studies.

In Table 1, only Lofgren and Zhu (2000) and Wang et al. (2014) treated all energy balance components in equation (1). This is unfortunate since it is necessary to know all terms of equation (1) together in order to understand the mechanisms of horizontal variability. This is because an increase of one component of energy balance must be compensated by a decrease of one or more components. By investigating a cause and effect relationship in this energy balance variation, there is a better chance in finding mechanism(s) behind such variation.

The whole lake surface was covered by the studies of Lofgren and Zhu (2000), Alcântara et al. (2010), Sima et al. (2013), Moukomala and Blanken (2017) while others focused on studies in a small area or along transect lines, or comparisons of properties in different regions. It is desirable to study the whole lake as this would provide us with information on the scale of spatial variability, ranging from a point scale to a lake-wide scale.

In Table 1, Lofgren and Zhu (2000) is the only study that worked on the whole lake and all energy balance components. The spatial resolution of monthly averages was 10 km. Because of this moderate resolution, they identified the geographical difference of the progress of a season as the main cause of spatial flux variability. Thus attention must be paid to finer scale variabilities (both in time and space) to capture variability due to air properties, lake geometry, waves, and currents.

1.3 Homogeneity of surface properties

Also, it can be noticed in Table 1 that there have been no studies that investigated the homogeneity of lake surface properties, except for Anttila et al. (2008) who applied semivariogram to analyze spatial variability of Chlorophyll-a and found that a point measurement is representative of only a small area because of patchiness of Chlorophyll-a. Note that the term "homogeneous" or "stationary" is a clearly defined concept in geostatistics and it requires rigorous analysis to judge homogeneity (see Section 3.2). Homogeneity of a surface is one of the requirements for accurate flux measurement (see, Section 5), and has been studied mainly over land surfaces, with a focus on vegetation, soil moisture, and surface temperature (e.g., Chen and Brutsaert, 1998, Cosh and Brutsaert, 1999). However, few investigations have been performed over lake surfaces, presumably because the scientific community has assumed uniform, i.e., spatially invariable, fluxes, which automatically guarantee homogeneous fluxes, casually without a proper analysis because lake surfaces are part of the water continuum.

1.4 Study purposes

The brief review of previous studies summarized above demonstrates fundamental lack of studies regarding the homogeneity of lake surface and horizontal flux variations. In particular, no previous studies have investigated all energy balance components over a whole lake surface at fine spatial and time resolutions. Also, no previous studies have investigated the mechanism responsible for the horizontal variability of various scales. Homogeneity has not been studied in lake environments. Thus, the purposes of this study were to investigate the occurrence, magnitude, and causes of horizontal flux and surface variability over a lake, and to clarify the influence of surface variability and homogeneity on flux measurements.

This paper is organized as follows. In section 2, the study area, Lake Kasumigaura, and data used in this study are introduced. In section 3, adopted methods are explained. In particular, surface energy balance components were determined by means of a bulk method applied to each 90 × 90 m pixel spanning the entire lake surface using remotely sensed surface temperatures and interpolated meteorological data as inputs. Application of the method using such a fine resolution was likely a first and allowed an estimation of the horizontally continuous fluxes required for the investigation of variability from a point scale to a lake-wide scale. In Section 4, the mechanism of horizontal variability and the homogeneity of surface temperature, T_s, are analyzed since T_s is the key surface variable for determining energy balance components. In section 5, possible problems during the determination of lake energy balance measurements are discussed based on results obtained for horizontal variability and surface homogeneity.

2 STUDY AREA AND DATA

2.1 Lake Kasumigaura

Lake Kasumigaura is the second largest lake in Japan and consists of Nishiura (172 km^2), Kitaura (36 km^2), Sotonasakaura (6 km^2), and connecting rivers. However, often, references to Lake Kasumigaura only include Nishiura. This naming convention is used in the following sections. An average depth of the lake is 4 m. Maximum depth of approximately 7 m occurs at the center of the lake. The lake has three coves, one to the west (Tsuchiura-iri), one to the north (Takahama-iri), and another small one cove (Edosaki-iri) in the southwest (Fig. 1).

The area surrounding the lake is generally flat with an altitude of approximately 30 m, while the lake surface altitude is 0.26 m. The exception is Mt. Tsukuba (877 m), the headwater region of the Kasumigaura watershed, located approximately 30 km to the north-west of the lake.

Unstable conditions prevail generally over Lake Kasumigaura throughout the day and regardless of season (Wei et al. 2016). During winter, clear skies are common. Therefore, to capture cloud-free satellite images of Lake Kasumigaura, data during winter were used (see Section 2.2).

2.2 Data

2.2.1 Meteorological data

Hourly or half-hourly data used in the analysis included wind speed, U (m/s), wind direction, relative humidity, and air temperature, T (°C), measured routinely at stations in and around Lake Kasumigaura. The location of the selected stations is provided in Fig. 1. A complete list of stations is provided in Sugita et al. (2014). In all, data from 21-25 stations for U, 11-16 stations for humidity, and 13-23 stations for T were used. For the analysis described below, specific humidity, q, (kg/kg) was determined at each station based on temperature and relative humidity.

2.2.2 Lake surface state

Wave height and wave period measurements from the Koshin observatory, located at the Kasumigaura River Office (KRO) at the center of Lake Kasumigaura (Fig. 1), were used to reveal surface lake conditions. Data and findings from special lake current observations organized by the KRO (INA Corporation 2008) were also utilized.

2.2.3 Satellite data products

The surface temperature, T_s (°C), of a 90×90-m pixel in the 2B03 product (ERSDAC 2003) created from thermal infrared images obtained from the Advanced Spaceborne Thermal Emission and Reflection Radiometer (ASTER) by applying radiometric, geometric and atmospheric corrections, and temperature-emissivity separation algorithm (Gillespie et al. 1998) were used to estimate surface fluxes by applying the bulk approach (Section 3.1). ASTER onboard the Terra satellite (ERSDAC 2003) has a polar, sun-synchronous orbit at approximately 705 km over the globe. The daytime satellite overpass time is approximately 10:30 am local time. The surface specific humidity, q_s, was also determined from the T_s data set.

To analyze surface fluxes for three cases (Cases I through III, see Table 2), three clear-sky scenes were selected. They differed mainly in wind speed, ranging from 0.85 to 7.19 m/s, and in lake surface state of wave height, wave period, and lake current (Table 3).

A comparison of T_s values from this product at the pixel corresponding to the Koshin observatory and in-situ measurements at this site using an infrared radiation thermometer yielded an RMS difference of 1.5°C for the three cases. In-situ measurements were recorded as 30-min averages (see Wei et al. 2016 for details of the measurements) such that the two averages prior to and following satellite overpass were interpolated in time to estimate T_s values for the comparison.

3 METHODS OF ANALYSIS

3.1 Determination of surface fluxes over Lake Kasumigaura

The entire surface of the lake was covered with 521 × 334 pixels, each with the size of 90 × 90 m. The pixels coincided exactly with surface temperature pixels. The components of equation (1) were estimated for each pixel by the procedure discussed below.

3.1.1 Interpolation of meteorological data over Lake Kasumigaura

Values of U, q, and T for each pixel at the time of satellite overpass were obtained through temporal and spatial interpolation, as follows.

Wind speed and direction measured at each station at a certain height z were first converted to U_{x10} and U_{y10}, the wind velocity components (m/s) at 10 m, by applying a profile equation under neutral condition (e.g., Brutsaert, 1982) with a roughness length estimated from surface land cover at each station using the method of Kondo and Yamazawa (1986). Details are explained in Ikura (2010). Note that the assumption of neutral stability results in 2-5% error in 10-m wind speed estimation for $z/L = -0.1$ to -10 (where L is the Obukhov length (m)) with $z = 5$ or 20 m and $z_0 = 0.11$ m. However, the following analysis was made mainly with non-dimensional variables (see Section 4.1), and thus errors in absolute values should not propagate into the final results too much. For q and T data, the height conversion was not applied because it would require surface fluxes at each meteorological station that were not available. Additionally, a sensitivity analysis indicated that conversion using the assumed flux values did not

produce markedly different results (Ikura 2010). The values were then interpolated linearly in time to determine U_{x10}, U_{y10}, q, and T at the time of satellite overpass.

The derived values of U_{x10}, U_{y10}, q and T were then interpolated spatially first, and U_{x10} U_{y10} of each pixel were then converted into the mean wind speed, U, and the wind direction. For interpolation, kriging (e.g., Webster and Oliver 2007) was used. Unlike other deterministic interpolation schemes such as inverse distance weighting, splines, or natural neighbor, it is a geostatistical technique which is based on variograms (see section 3.2) and uses statistical properties and spatial relationships of samples to create a model to interpolate sampled points. Advantages of kriging compared with others are its flexibility in its determination of weights and availability of means to evaluate the magnitude of the estimation error (Kitanidas 1997), and therefore it is popular and used commonly in many fields including hydrology.

3.1.2 Bulk equations for estimating sensible and latent heat fluxes

To determine L_eE and H, bulk equations were applied to each pixel as they are virtually the only choice available in the present context and purposes. Although there are many empirical equations to estimate E of a lake (e.g., Majidi et al. 2015), there are not many options for estimating H. Also, bulk equations are more appealing as they can be derived from profile equations which were established on the basis of similarity theory and have been tested in numerous field experiments. The approach is essentially the same as that adopted by Sugita et al. (2014) for the E estimation at Lake Kasumigaura and by Lofgren and Zhu (2000) for the energy balance estimation with a 10-km resolution for the Great Lakes. Sugita et al. (2014) indicated that hourly E values from the eddy correlation method compared well (RMS error = 0.03 mm/h) with those from equations (2)-(5) over a 5-year period at the Koshin observatory.

The bulk equations can be expressed, as follows:

$$L_eE = \rho L_e C_E U \left(q_s - q\right), \tag{2}$$

$$H = \rho c_p C_H U \left(T_s - T\right), \tag{3}$$

where C_E and C_H are the bulk transfer coefficients for water vapor and heat, respectively, and c_p is the specific heat of air at constant pressure (J/kg/K).

Values of C_{EN} and C_{HN}, bulk coefficients under neutral conditions for a reference height of 10 m, were determined over Lake Kasumigaura. Their functional dependence on neutral wind speed U_{10N} (m/s) at 10 m, based on measurements at the Koshin observatory, was provided by Wei et al. (2016), as follows:

$$C_{EN} = \left(b_{E1} / U_{10N}\right) \exp\left[-\left(\ln U_{10N} - b_{E2}\right)^3\right] + \left(b_{E3} + b_{E4} U_{10N}\right), \quad (4)$$

$$C_{HN} = \left(b_{H1} / U_{10N}\right) \exp\left[-\left(\ln U_{10N} - b_{H2}\right)^3\right] + \left(b_{H3} + b_{H4} U_{10N}\right). \quad (5)$$

The coefficients have values of $b_{E1} = 9.1 \times 10^{-4}$, $b_{E2} = 2.2 \times 10^{-1}$, $b_{E3} = 1.1 \times 10^{-3}$, and $b_{E4} = -1.5 \times 10^{-5}$ for equation (4); and $b_{H1} = 2.1 \times 10^{-3}$,; and $b_{H2} = 2.8 \times 10^{-1}$, $b_{H3} = 9.1 \times 10^{-4}$, and $b_{H4} = 1.6 \times 10^{-5}$ for equation (5).

Equations (4) and (5) were optimized for fluxes measured at the center of the lake. When estimating the distribution of fluxes over the entire lake surface, they may not be appropriate near the shoreline where the influence of surrounding land surfaces may be important. Such influence has been studied extensively in the past within the framework of development for the internal boundary layer (see, e.g., Brutsaert 1982). From these studies, the empirical equation of Kondo (1982) was adopted for considering advection effects near the shore. The result was obtained by solving the diffusion equation of water vapor numerically for a step change of surface humidity without a change in surface roughness at the shoreline. Incoming humidity, advected by winds having a logarithmic profile, was assumed to be vertically constant. This type of solution was chosen because the wind condition surrounding Lake Kasumigaura was not impacted greatly by small elevation differences between the lake's surface and the surrounding areas (Shintani 2008, Wei et al. 2016). Also, specific humidity above the land's surface was not very different from that above the lake. Therefore, for the distance from the shoreline along the wind direction $x_{up} \geq 1$ km, equations (4) and (5) were used. For $x_{up} < 1$ km, $C_{HN} = C_{EN} = 1.994 x_{up}^{-0.1}$ was used instead.

C_{EN} and C_{HN} were then converted into C_E and C_H by multiplying

$$\frac{C_H}{C_{HN}} = \frac{C_E}{C_{EN}} = \left[1 - \Psi_H(\zeta) / \ln(z / z_{0h})\right]^{-1} \left[1 - \Psi_M(\zeta) / \ln(z / z_0)\right]^{-1} \quad (6)$$

in which Ψ is the stability correction function of the stability parameter $\zeta = z / L$. The subscripts H and M stand for heat and momentum, respectively. The symbols z_{0h} and z_0 are the scalar roughness length for sensible heat and momentum roughness length, respectively. The details of estimation of (6) for three cases are explained in Section 1 of Supplementary material.

3.1.3 Other energy balance components

Incoming and reflected short-wave radiation, R_{sd} and R_{su}, respectively, and incoming long-wave radiation, R_{ld}, were assumed constant throughout the lake's surface. Values obtained from the Koshin Observatory were employed because a preliminary analysis with R_{sd} measurements at nine locations and R_{ld} measurements at two locations surrounding the lake supported this assumption. Hiyama et al. (1995) indicated uniform incoming radiation under clear sky conditions over an area of 16 × 16 km in this region, which also supports the assumption.

Outgoing long-wave radiation, R_{lu} (W/m^2), was determined from T_s by:

$$R_{lu} = \varepsilon \sigma T_s^4 \quad (7)$$

where ε is the broadband emissivity over wavelengths of R_{lu} (approximately 3-100 μ m) and σ is the Stefan-Boltzmann constant (W/m^2/K^4). ε=1.0 was assumed because of the uncertainty of the ε value over a lake surface where the wind speeds, turbidity and incident angles play a role. Note that changing ε value from 1.0 to 0.97 results in only 2.2-2.8 W/m^2 (0.67-0.8%) difference in R_n.

Finally, the heat flux going into a lake water body, G, was obtained as the residual of the surface energy balance equation (1):

$$G = R_n - L_e E - H. \quad (8)$$

Here, it should be remembered that errors in R_n, L_eE, and H are lumped together into the G term. This point will be discussed in Section 4.1

3.2 Semivariogram

To investigate whether or not a variable is homogeneous in space, applying a common technique in geostatistics using a semivariogram is convenient (e.g., Wackernagel 1995, Webster and Oliver 2007, Sarma 2009). Note that "stationarity" is used generally to indicate a homogeneous condition in geostatistics. However, it implies time-dependent processes so an alternative term "homogeneity" (Brutsaert 1998) is used in the following discussion.

The semivariogram in a two-dimensional field is defined as:

$$\gamma\left(\Delta x, \Delta y\right) = \frac{1}{2n}\sum_{i}^{n}\left[Z\left(x_i + \Delta x, y_i + \Delta y\right) - Z\left(x_i, y_i\right)\right]^2 \tag{9}$$

where $Z(x, y)$ is a random variable at position (x, y). The symbols Δx and Δy represent components of a separation distance vector in the x- and y-direction, respectively. Thus, the semivariogram is half the variance of Z separated by a distance $(\Delta x, \Delta y)$. Here, the absolute position (x_i, y_i) is not an issue and only the separation distance $(\Delta x, \Delta y)$ is relevant.

Equation (9) can be further simplified as:

$$\gamma\left(h\right) = \frac{1}{2n}\sum_{i}^{n}\left[Z\left(x_i + h\right) - Z\left(x_i\right)\right]^2 \tag{10}$$

if the variability is isotropic. In such a case, it is called an omnidirectional semivariogram. When anisotropy is suspected, a semivariogram for a specific direction is analyzed. The result is referred to as a directional semivariogram. In the following analysis, the direction is specified as the angle ± tolerance. The symbol h is the separation distance (m) referred to as the lag and it is expected that γ increases as h increases because the surface variables, Z, at two nearby locations are likely similar and related but becomes less similar as h increases. In this case, Z is spatially dependent. If Z is homogeneous, γ stops increasing eventually and becomes a constant (ideally it is the variance, σ^2) at a certain separation distance. The distance and the constant are, respectively, referred to as the range and the sill. The range indicates the limit of spatial dependence beyond which Z values are spatially independent. Thus, the existence of a sill can be used to diagnose surface homogeneity (see, e.g., Brutsaert 1998, Cosh and Brutsert 1999). Note that the homogeneity in this context is more exact when referred to as a second-order homogeneity or a weak homogeneity (stationarity), indicating that the first and second moments only depend on the separation distance and not on the absolute position. In the following discussion, a simple term of homogeneity is used.

4 CHARACTERISTICS OF LAKE SURFACE ENERGY BALANCE AND SPATIAL VARIABILITY

4.1 Surface fluxes and relevant variables

Table 2 lists a summary of surface energy balance components and general meteorology for the three selected cases. As mentioned previously, the three cases differ mainly in their wind speeds. A weak wind condition is represented by Case II (7 December 2007), a windy condition by Case III (1 January 2009), and an intermediate wind condition by Case I (21 November 2007).

A large percentage (78-92%) of R_n was distributed to G, while L_eE and H were both minor components. Thus, in these three cases, the lake water body was heated as a result of the surface energy balance. However, such is not typical in the November-January period when, on average, energy is lost from lake water to the atmosphere (Sugita et al. 2014). The difference resulted likely from the fact that the three cases were cloud-free, clear days with strong sunshine.

Note that in this analysis, errors, ε_E, in the energy balance components lumped together into G in equation (8) were assumed to be negligible. Although there was no confirmation that this assumption was acceptable at the time of the study, it can be argued that ε_E did not influence greatly the estimation of G in light of results indicating that L_eE and H were minor components in equation (8). The majority of ε_E is expected to result from L_eE and H. Also, a preliminary study (Kawade, 2019) which compared the G values with the storage changes in the lake water body calculated from the time change of temperature profiles measured at the Koshin observatory indicated a good agreement (R^2=0.78 with a fitted linear equation through the origin of y=0.78x) for the 1214 data points. The scatter was suspected due to the lake bottom heat flux and advected energy by the lake current.

Figure 2 indicates the spatial distribution of surface fluxes R_n, G, L_eE, and H together with the relevant variables for Case I. Corresponding figures for Cases II and III are shown in Figs. S1 and S2. In each figure, a variable X was converted into a scaled variable, as follows:

$$Y = \frac{X - \overline{X}}{s_X} \tag{11}$$

in which the overbar denotes the spatial average over Lake Kasumigaura and s_X is the standard deviation of X. Use of the scaled variable Y instead of X allows easy comparison of the characteristics on the spatial distribution of fluxes and meteorological variables having a different magnitude.

Clear from Fig. 2 is that an organized pattern of distribution is visible for L_eE, H, and G, while it is less clear for R_n. For example, higher values of L_eE as compared to the spatial mean are noticeable surrounding the northeastern portion of the lake. Lower values were determined in the western end in Tsuchiura-iri and in southern portions of the lake. Similar patterns can also be noted in the other two cases (Figs. S1-S2). The presence of variable fluxes such as these is also observed in the statistics (Table 2). The coefficient of variation (CV) of R_n was 0.01 for all three cases, while that of L_eE and H was in the range of 0.23-0.39. The kurtosis was quite large, reflecting stretched tails in the probability distribution curve. The positive skewness for L_eE and H indicates that the stretched tails were skewed toward larger values. A closer look at the data indicates that these organized patterns originated mainly from surface temperature values, as further discussed in Section 4.2.

To give another statistical indicator of the distribution characteristics, two types of a center for the spatial mean are provided in Fig. 2 (and also in Figs. S1-S2). One is a simple geographical center calculated by:

$$z_1(x, y) = \left(\frac{\sum x_i}{n}, \frac{\sum y_i}{n}\right) \tag{12}$$

where z_1 is a location vector with its components of x- and y- coordinates; x_i and y_i are the x and y coordinates of the i-th pixel within the lake, and n is the total grid number. x is provided in the east-west direction and y in the north-south direction. Also indicated is the weighted geographical center, centroid, given by:

$$z_2(x, y) = \left(\frac{\sum f_i x_i}{\sum f_i}, \frac{\sum f_i y_i}{\sum f_i}\right) \tag{13}$$

where f is the magnitude of the target variable of each figure. For example, in Fig. 2(c), $f = L_e E$. For Case I, z_2 is located to the east of z_1 for L_eE and H, the same as in Case III. For Case II (Fig.S1), z_2 is aligned to the west for L_eE, reflecting higher values in Tsuchiura-iri.

The organized distribution identified above can be scrutinized by comparing the horizontal distribution of fluxes with that of variables in the bulk equations (2)-(3). These variables are shown in panels (e) - (k) of Fig. 2. Such comparisons revealed immediately that the horizontal distribution was determined largely by the vertical concentration differences, $(q_s - q)$ and $(T_s - T)$, or the wind speeds, U. For Case I (Fig. 2), both the concentration differences and U were equally important. This was also the circumstance for Case III, while concentration differences were the main factor in determining the flux distribution for Case II under weak wind conditions (Fig. S1). On the other hand, vertical concentration differences came from T or q (Cases I and II) and T_s or q_s (Case III). The distribution of C_E and C_H did not influence much of the flux distribution. The result is natural since C_E and C_H do not change to a great extent.

Figure 3 indicates horizontal variation for T_s, $(T_s - T)$, H, U, and C_H, scaled by (11), for Case III as an example, along the three cross-sectional lines (see Fig.1) in Lake Kasumigaura. In the figure, a small-scale fluctuation of H on the order of 10^2 m, independent of the lake-scale variation explained above, is noticeable. Such fluctuation corresponds very well to those of $(T_s - T)$. The same feature can be observed for L_eE and $(q_s - q)$; and for the other two cases (not shown). A comparison of the variation of $(T_s - T)$ and that of T_s confirmed that such a small-scale fluctuation originated largely from T_s.

T_s at a fixed point should change continuously in time, depending on the surface energy balance and the lake current and/or waves. Thus, over an area or along a cross-section, the horizontal variability of T_s at any particular moment as realized from a snapshot of the ever-changing T_s at each point is likely. As a result, the fluctuations of T_s observed in Fig. 3 suggest the presence of some sort of structure of the scale of 10^2

m. However, a phenomenon at a horizontal scale < 90 m cannot be detected by the ASTER sensor. Thus, it is possible that finer scale fluctuations not observed in this study exist. Indeed, the wavelength was 10-20 m as estimated from the significant wave period (Table 3) and an assumed depth of 4-7 m; so it is possible that there was a fluctuation in this scale. This point will further be studied in Section 4.2 by means of a semivariogram analysis.

Distinctive values can be observed near coastal lines. First, C_H was larger than in open water for $x_{up} < 1$ km as a result of its treatment to include the influence of internal boundary layer development when the wind was blowing toward the lake. The condition resulted in higher values of H for the horizontal extent, $x_{up} < 1$ km.

Second, H, T_s, and $(T_s - T)$ were found to be much higher to the west near the A point than averages along the A-A' line. The A point was located near the western end of Tsuchiura-iri where the depth ≤ 1 m. On the other hand, near the northeastern end of the B-B' line, those variables were smaller than the averages. Such distinctive characteristics, different from the averages, were likely due to local conditions near the shoreline. One such local condition was an extended shallow water zone offshore from the shorelines. Water in such a shallow zone likely becomes detached and isolated from the main lake and induces a local energy balance that could be different from the type that occurs in open water. However, an inspection of Fig. 3 and equivalent figures for Cases I and II (not shown) did not reveal a clear, consistent relationship between the depth and the nature of horizontal variations. The result occurred likely because the depth and other factors caused distinctive variation near the shoreline. The intermittent presence of reed communities and/or breakwaters near the shoreline may have played a role. These communities act as barriers for water movement offshore to the shoreline.

Another possibility is the influence of an advected water body with a different temperature. An observation at the Koshin observatory in Case III (Table 3) indicates that the water temperature was lower at a deeper depth. Therefore, if local upward water flow exists, the surface temperature tends to become lower. However, available lake current information (INA Corporation 2008; see also Fig. S3) indicates that water circulates mostly horizontally and vertical circulation only occurs at limited locations in Lake Kasumigaura. At any rate, it is quite clear that careful treatment of the surface energy balance consideration is necessary near the shoreline.

4.2 Surface temperature

Since surface temperature plays a major role in energy balance variation in Lake Kasumigaura, it was further investigated. In general, spatial differences in the absolute values of T_s (and q_s) were small. For the three cases, the standard deviation, s , of T_s was 0.6-0.7°C with CV = 0.05-0.10 (Table 2). On the other hand, kurtosis was large, reflecting longer tails in the probability distribution curve. The result implies the presence of outliers. A comparison with Fig. 2(k) indicates that such outlier values were near the shoreline (also see Figs. S1(k) and S2(k)). These outlier values propagated into the (T_s - T) and H fields and resulted in outlier flux values near the shoreline (Fig. 2(d)), as mentioned in Section 4.1. Skewness was positive such that the right-hand tail (higher T_s) was longer than the left-hand tail and the outlier, T_s, with higher values, was more pronounced particularly in Cases II and III.

Figure 4 provides the experimental omnidirectional semivariogram of Lake Kasumigaura as a function of the separation distance, h, for Case I. Corresponding figures for Cases II and III are provided in Figs. S4-S5. The semivariogram was calculated up to a separation distance of approximately 10-11 km, which is 1/3 of the diagonal extent of the dataset. The derived semivariogram was then normalized by the variance so that features of the different semivariograms could be compared with one another.

First, it is clear from Fig. 4 that the y-intercept is not zero. This is called the nugget effect and indicates (i) fluctuations at a scale smaller than horizontal resolution of the data (= 90 m) or (ii) the presence of random observational error. The first cause of the nugget effect is consistent with an assessment of the small-scale fluctuation of T_s noted in Section 4.1.

Figure 4 also indicates that a sill does not exist. Therefore, T_s was judged nonhomogeneous for the examined distance for Case I. This result was the same as for Case III. In Case II, on the other hand, a sill (≒1.06) and a range (≒3.5 km) were well defined. Therefore, T_s can be considered homogeneous over the surface of Lake Kasumigaura.

The difference in these three cases suggests that only under calm conditions, T_s can be considered homogeneous over the majority of the surface of Lake Kasumigaura. Under windy conditions, the lake current likely developed for certain directions and

enhanced waves (Table 3; see also Fig. S3.) causing directional horizontal mixing of surface water, resulting in first and second moments that depended not only on the separation distance but also on the absolute position.

In these figures, directional semivariograms are also shown for six directions. Ranges for various directions for the three cases are summarized in Table 4. Obviously, the T_s variation was anisotropic. Depending on the direction, different sills were obtained. For certain directions, a sill did not exist. For example, a sill exists in the directions of 60-120° (general N-S directions) and T_s can be considered homogeneous for Case I even though it was judged to be non-homogeneous in the omnidirectional semivariogram. Also, a hole effect and a nested structure (e.g., Webster and Oliver, 2007; Sharma, 2009) are noticeable for certain directions. The hole effect observed as a bump in the semivariogram (corresponding to a hole in the covariance) is an indication of natural fluctuations in the semivariogram arising from repetition in the process. The nested structure suggests the presence of variations at different scales and the resulting semivariogram is thought to be composed of plural semivariograms representing each scale. For example, sills were found at 5-8 km for the direction of 60-120°, beyond which γ remained constant. However, γ began increasing again at h = 9.3 - 10.3 km and reflected the variability of the larger scale. This nested structure was also obvious in the omnidirectional semivariogram.

For Case I and III (windy conditions), the longest range (8 km) appeared in the direction of 60°. As observed from Fig. 1, this is the direction where a longer fetch is available in the eastern portion of Lake Kasumigaura. Thus, it is likely an indication that closeness to the shorelines affects T_s variability and causes a nonhomogeneous distribution. Indeed, directional semivariograms (Table 5) of the T_s data within a circle in Tsuchiura-iri near the shoreline (Fig.1) did not sill, with the exception of Case II. In contrast, corresponding semivariograms in Koshin (away from the shoreline) indicated the presence of range and, thus, homogeneity.

Finally, it should be noted that the findings obtained above for T_s should also be applicable for q_s since q_s is a monotone increasing function of T_s.

5 IMPLICATIONS FOR LAKE FLUX MEASUREMENTS

The findings presented above raise certain questions regarding the validity of common flux measurement practice and therefore it merits discussion.

The main concern in flux measurements is generally an adequate fetch in scientific communities. A setting often adopted for lake energy balance measurements is to install a tower over the water's surface close to shorelines (e.g., Ikebuchi et al. 1988, Ataktürk and Katsaros 1999, Xiao et al. 2013, Wang et al. 2014). In this setting, data measured when the wind direction is from open water were selected and used to fulfill fetch requirements with the hope that they represent the open water surface of lakes. The above analysis indicates that these tower settings are not necessarily acceptable, at least in Lake Kasumigaura, since surface variables near coastal lines (< 1 km) are clearly different from those observed offshore. Moreover, the T_s field was determined to be non-homogeneous, particularly near shorelines. Therefore, only satisfying the fetch requirements may not guarantee an accurate surface flux.

To measure accurate fluxes by means of micrometeorological methods, the surface flux must be statistically homogeneous (Brutsaert 1998), and the discussion could be made in a more formal manner by considering specific requirements to fulfill this condition. Specific criteria for satisfying this condition were also discussed in Brutsaert (1998). Among listed criteria, those relevant to the present discussion can be rephrased as follows: (i) the surface should be statistically homogeneous, (ii) the fetch, l_f, of a homogenous surface should be larger than the length scale of homogeneity specified by the range l_r, and (iii) the source area scale l_s to indicate the extent of the upwind surface sources contribution to the measured flux, should be larger than l_r. They ensure adequate sampling of surface variability. Additionally, a common fetch requirement states that (iv) l_f should be larger than l_s. Criteria (ii) - (iv) can be summarized as $l_f > l_s > l_r$.

If a measurement height of z = 10 m, a typical stability of $z/L = -0.015$, and a roughness length $z_0 = 10^{-4}$ m over Lake Kasumigaura (Wei 2013) are assumed, application of a footprint analysis (Kljun et al. 2015) indicates that approximately 90% of the fluxes originate from within the source area, with an upwind distance of l_s=1.1 km. With this value in mind, we can consider two cases for the flux tower setting. The first case is an actual flux station established at the Koshin Observatory (Fig. 1; Sugita et al. 2014, Wei et al. 2016) at the center of Lake Kasumigaura. For a dominant wind direction of north to northeast, the distance to the shoreline is on the order of 3-5 km. The surface temperature field in this direction was judged to be homogeneous by using a semivariogram analysis with a range of l_r= 250-400 m and $l_f \geqq 1.3$ km (Table 5). Thus, $l_f > l_s > l_r$ which satisfies criteria (i)- (iv). Therefore, as expected, flux

measurements at the Koshin Observatory near the center of the lake satisfy all of the criteria and ensure that measured atmospheric flow samples surface variability.

The second case is a hypothetical flux station in Tsuchiura-iri near the coast. The criteria (i)- (iv) were satisfied only for Case II with l_s = 1.1 km, $l_f \geqq$ 1.3 km, and l_r = 350 m. On the other hand, the range does not exist for Cases I and III (Table 5). Therefore, fluxes from this station may not always be as accurate as those from the Koshin Observatory.

The discussion provided above illustrates clearly the need for further consideration of our current practice. In particular, careful attention must be paid not only to the atmospheric portion (, i.e., a sufficient fetch) but also to surface conditions (i.e., homogeneity) in order to interpret or make flux measurements. Also, note that this is not necessarily limited to flux measurements. For example, surface temperatures have often been investigated by means of infrared radiance images produced by satellite remote sensing (e.g., Sugita and Brutsaert 1993). A comparison with in situ measurements is made generally from such data for their validation. Based on the findings above, it is also clear that care must be paid to the horizontal position of in situ measurements. They should be obtained further from the shoreline. Also, measurements should be obtained at a location where the homogeneous condition is satisfied over the extent of at least the size of satellite pixels.

6 CONCLUSIONS

Results obtained in this study can be summarized below on each of the specific questions raised in the introduction section.

6.1 Are surface energy balance components uniform in Lake Kasumigaura?

No, they are not. In a relative sense, the latent heat flux, L_eE, and sensible heat fluxes, H, and the heat flux going into lake water, G, differed horizontally regardless of wind condition much more than the net radiation R_n. The horizontal variation of heat fluxes consisted of two scales, the lake scale (on the order of 10^3 -10^4 m) and a finer scale on the order of 10^2 m. Additionally, fluxes near the shoreline were quite different from those offshore.

6.2 What are the causes of horizontal variability?

Larger scale variation was controlled mainly by the horizontal variation of air temperature or specific humidity (for three cases) and wind speed (with the exception of Case II under weak wind conditions), while a finer scale variation was due to the horizontal fluctuation of surface temperature. Distinct fluxes near the shoreline were caused by the influence of incoming air from land surfaces (when the wind direction was from the land to the lake) and shallow water depth.

6.3 Is surface temperature homogeneous?

It was found that surface temperature was found homogeneous only for Case II under calm conditions. For Cases I and III, the surface temperature was homogenous only for certain directions having a longer fetch. These differences between calm and windy conditions were caused likely by the directional mixing of surface water due to the lake current together with waves developing under windy conditions. Overall, the surface temperature was quite different near the shoreline from that in the central portion of Lake Kasumigaura.

6.4 Where should we establish a flux tower?

It was shown that the station near the coastline could violate the requirement of surface homogeneity, even when the fetch requirements were satisfied. In contrast, the station located near the center portion of the lake satisfied both criteria. Thus, this location is expected to produce more accurate fluxes. Overall, air properties, as well as surface conditions, must be considered carefully in many aspects of lake studies.

The above conclusions were derived based on the anayses of three cases with different wind speeds under clear sky condition during winter months. Thus applicability of the results to other conditions should be verdified with more studies under range of conditions.

Acknowledgements

I acknowledge Ikura, H., a former student at the University of Tsukuba, for his preliminary analysis of lake surface temperature by means of remote sensing methods that lead to the present analysis. I also thank the Kasumigaura River Office of the Kanto Regional Development Bureau, Ministry of Land, Infrastructure, Transport, and Tourism of Japan for allowing our measurements at the Koshin Observatory and for providing us with miscellaneous data sets. Meteorological data used in the analysis were obtained from the Kasumigaura River Office, by the Lake Kasumigaura Water Research Station of the National Institute for Environmental Studies, by the Japan Meteorological Agency, by Ibaraki Prefecture, and by the Hyakuri Air Base of the Japan Air Self-Defense Force. Constructive comments of two reviewers and the associate editor Guillaume Thirel which helped to improve the quality of the manuscript are much appreciated.

Funding

This work was supported and financed, in part, by Japan Society for the Promotion of Science [Grant Number KAKENHI 15K01159]. Parts of this study were conducted while MS was at Kyoto University as a visiting professor.

REFERENCES

Alcântara, E.H. et al., 2010. Remote sensing of water surface temperature and heat flux over a tropical hydroelectric reservoir. *Remote Sensing of Environment*, 114, 2651-2665. doi: 10.1016/j.rse.2010.06.002. doi: 10.1007/s10661-007-9904-y

Anttila, S. et al., 2008. A feasible method to assess inaccuracy caused by patchiness in water quality monitoring. *Environmental Monitoring and Assessment*, 142, 11-22. doi: 10.1007/s10661-007-9904-y

Ataktürk, S.S. and Katsaros, K.B., 1999. Wind stress and surface waves observed on Lake Washington. *Journal of Physical Oceanography*, 29, 633-650. doi: 10.1175/1520-0485(1999)029<0633:WSASWO>2.0.CO;2

Blanken, P. D. et al., 2003. Enhancement of evaporation from a large northern lake by the entrainment of warm, dry air. *Journal of Hydrometeorology*, 4, 680-693. doi: 10.1175/1525-7541(2003)004<0680:EOEFAL>2.0.CO;2.

Brutsaert, W., 1982. *Evaporation into the atmosphere.* Boston: D Reidel Publishing Company

Brutsaert, W., 1998. Land-surface water vapor and sensible heat flux: spatial variability, homogeneity, and measurement scales. *Water Resources Research*, 34, 2433-2442. doi: 10.1029/98WR01340.

Chen, D. and Brutsaert, W., 1998. Satellite-sensed distribution and spatial patterns of vegetation parameters over a tallgrass prairie. *Journal of the Atmospheric Sciences*, 55, 1225-1238. doi: 10.1175/1520-0469(1998)055<1225:SSDASP>2.0.CO;2.

Cole, J.J., et al., 2007. Plumbing the global carbon cycle: integrating inland waters into the terrestrial carbon budget ecosystems. *Ecosystems*, 10, 172-185. doi: 10.1007/s10021-006-9013-8.

Cosh, M.H. and Brutsaert, W., 1999. Aspects of soil moisture variability in the Washita '92 study region. *Journal of Geophysical Research*, 104, D16, 19,751-19,757. doi: 10.1029/1999JD900110.

ERSDAC (Earth Remote Sensing Data Analysis Center), 2003. *ASTER reference guide* version 1.0 [online]. Geological Survey of Japan. Available from: https://unit.aist.go.jp/igg/rs-rg/ASTERSciWeb_AIST/en/documnts/ [Accessed 22 May 2018].

Foken, T., 2008. *Micrometeorology*. Berlin: Springer.

Gillespie, A. et al., 1998. A temperature and emissivity separation algorithm for Advanced Spaceborne Thermal Emission And Reflection Radiometer (ASTER) images. *IEEE Transactions on Geoscience and Remote Sensing*, 36, 1113–1126. doi: 10.1109/36.700995.

Heikinheimo, M. et al., 1999. Momentum and heat fluxes over lakes Tämnaren and Råksjö determined by the bulk-aerodynamic and eddy-correlation methods. *Agricultural and Forest Meteorology*, 98-99, 521-534. doi: 10.1016/S0168-1923(99)00121-5.

Hemond,H.F. and Fechner-Levy, E.J., 2000. *Chemical fate and transport in the environment.* 2nd ed. London: Academic Press.

Hiyama, T., Sugita, M. and Kayane, I., 1995. Variability of surface fluxes within a complex area observed during TABLE 92. *Agricultural and Forest Meteorology*, 35, 189-207. doi: 10.1016/0168-1923(94)05074-G

Hoverman, J. T. and Johnson, P. T.J., 2012. Ponds and lakes: a journey through the life aquatic. *Nature Education Knowledge,* 3, 17.

Huang, C., et al., 2019. Long-term variation of phytoplankton biomass and physiology in Taihu lake as observed via MODIS satellite. Water Research 153, 187-199. doi: 10.1016/j.watres.2019.01.017.

Ikebuchi, S., Seki, M., and Ohtoh, A., 1988. Evaporation from Lake Biwa. *Journal of Hydrology*, 102, 427–449. doi:10.1016/0022-1694(88)90110-2

Ikura, H. 2010., Estimation of evaporation distribution over Lake Kasumigaura using satellite data. MS thesis, Graduate School of Life and Environmental Sciences, University of Tsukuba. (in Japanese)

INA Corporation, 2008. *Report on the investigation of lake current of Lake Kasumigaura*. Tokyo: INA Corp. (in Japanese)

ILCF (International Lake Committee Foundation), 2019. *Data from: World Lake Database* [dataset]. Available from: http://wldb.ilec.or.jp/ [Accessed 1 April 2019].

Kawade, M., 2019. Spatial variation of heat storage in Nishiura, Lake Kasumigaura. BS Thesis, College of Geoscience, University of Tsukuba.

Kawamura, S. and Fukushima, T., 2018. Residents' concerns about lake uses and environments: a comparative study of Lakes Kasumigaura, Suwa, and Biwa in Japan. *Limnology*, 19, 101-113. doi: 10.1007/s10201-017-0523-1.

Kennedy, R.H. and Walker W., 1990. Reservoir nutrient dynamics. In: K.W. Thornton, Kimmel, B.L., and Payne, F.E., eds. *Reservoir limnology*: ecological perspectives. New York: Wiley-Interscience, 109-131.

Kitanidis, P.K., Introduction to geostatistics: applications in hydrogeology, Cambridge: Cambridge University Press.

Kljun, N., et al., 2015. A simple two-dimensional parameterization for Flux Footprint Prediction (FFP). *Geoscientific Model Development*, 8, 3695-3713, 2015. doi: 10.5194/gmd-8-3695-2015.

Kondo, J., 1982. *Science on the atmospheric boundary layer.* Tokyo: Tokyo-do Syuppan, Co. Ltd. (in Japanese)

Kondo, J. and Yamazawa, H., 1986. Aerodynamic roughness over an inhomogeneous ground surface. *Boundary-Layer Meteorology.* 35, 331-348. doi: 10.1007/BF00118563.

Li, Z., et al., 2015. Long-term energy flux and radiation balance observations over

Lake Ngoring, Tibetan Plateau. *Atmospheric Research*, 155, 13-25. doi: 10.1016/j.atmosres.2014.11.019.

Lofgren, B. M. and Zhu, Y., 2000. Surface energy fluxes on the Great Lakes based on satellite-observed surface temperatures 1992 to 1995. *Journal of Great Lakes Research*, 26, 305-314. doi: 10.1016/S0380-1330(00)70694-0.

Mahler, Y. and Assouline, S., 1993. Evaporation from Lake Kinneret: 2. Estimation of the horizontal variability using a two-dimensional numerical mesoscale model. *Water Resources Research*, 29, 911-916. doi: 10.1029/ 92WR02433.

Majidi, M. et al., 2015. Estimating evaporation from lakes and reservoirs under limited data condition in a semi-arid region. Water Resources Management, 29, 3711-3733. doi: 10.1007/s11269-015-1025-8

Moukomla, S. and Blanken, P. D., 2017. The estimation of the North American Great Lakes turbulent fluxes using satellite remote sensing and MERRA reanalysis data. *Remote Sensing*, 9, 141. doi: 10.3390/Rs9020141.

Notaro, M., et al., 2013. Influence of the Laurentian Great Lakes on regional climate. *Journal of Climate,* 26, 789-804. doi: 10.1175/JCLI-D-12-00140.1.

Nordbo, A., et al., 2011. Long-term energy flux measurements and energy balance over a small boreal lake using eddy covariance technique. *Journal of Geophysical Research: Atmosphere*, 116, D02119. doi: 10.1029/2010jd014542.

Rahaghi, A. I., et al., 2019. Surface water temperature heterogeneity at sub-pixel satellite scales and its effect on the surface cooling estimates of a large lake: Airborne and remote sensing results from Lake Geneva. *Journal of Geophysical Research: Oceans*, 124, 635-651. doi:10.1029/2018JC014451

Rouse, W. R., et al., 2008. An investigation of the thermal and energy balance regimes of Great Slave and Great Bear Lakes. *Journal of Hydrometeorology*, 9, 1318-1333. doi: 10.1175/2008JHM977.1.

Sarma, D.D., 2009. *Geostatistics with applications in earth sciences*. 2nd ed., Dordrecht: Springer.

Shintani, T., 2008. Numerical estimation of wind and wave fields for lake environment using meso–scale atmospheric model WRF. *Journal of Japan Society of Civil Engineers, Ser. B1*, 52, 1237–1242. doi:10.2208/prohe.52.1237 (in Japanese)

Sills, D.M.L., et al., 201. Lake breezes in the southern Great Lakes region and their influence during BAWS-Met 2007. *Atmospheric Chemistry and Physics*, 11, 7955-7973. doi: 10.5194/acp-11-7955-2011.

Sima, S., et al., 2013. Mapping surface temperature in a hyper-saline lake and investigating the effect of temperature distribution on the lake evaporation. *Remote Sensing of Environment*, 136, 374-385. doi: 10.1016/j.rse.2013.05.014.

Stull, R.B., 1988. *An introduction to boundary layer meteorology*. Dordrecht: Kluwer Academic Publishers.

Sugita, M., *et al.*, 2014. Evaporation from Lake Kasumigaura: annual totals and variability in time and space. *Hydrological Research Letters*, 8, 103-107. doi:10.3178/hrl.8.103

Sugita, M. and Brutsaert, W., 1993. Comparison of surface temperatures derived from satellite observations with ground truth during FIFE. *International Journal of Remote Sensing*, 14, 1659-1676. doi:10.1080/01431169308953993

Tanny, J., et al., 2008. Evaporation from a small water resourvoir: Direct measurements and estimates. *Journal of Hydrology*, 351, 218-229. doi; 10.1016/j.jhydrol.2007.12.012.

Wackernagel, H., 1995. *Multivariate geosratistics*. Berlin: Springer-Verlag.

Wang, W., et al., 2014. Temporal and spatial variations in radiation and energy balance across a large freshwater lake in China. *Journal of Hydrology* 511, 811-824. doi:10.1016/j.jhydrol.2014.02.012.

Webster, R. and Oliver, M.A., 2007. *Geostatistics for environmental scientists.* 2nd ed. Chichester: John Wiley & Sons Ltd.

Wei, Z., 2013. Estimation of surface fluxes using bulk transfer methods over lake surface: an example of Lake Kasumigaura. MS Thesis, Graduate School of Life and Environmental Sciences, University of Tsukuba.

Wei, Z., Miyano, A., and Sugita, M., 2016. Drag and bulk transfer coefficients over water surfaces in light winds. *Boundary-Layer Meteorology*, 160, 319–346, doi: 10.1007/s10546-016-0147-8

Wetzel, R.G., 1983. *Limnology*, 2nd ed. Philadelphia: Saunders College Pub.

Woolway, R.I. and Merchant, C.J., 2018. Intralake heterogeneity of thermal responses to climate change: A study of large Northern Hemisphere lakes. *Journal of Geophysical Research: Atmospheres*, 123, 3087–3098. doi:10.1002/2017JD027661

Xiao, W., et al., 2013. Transfer coefficients of momentum, heat and water vapour in the atmospheric surface layer of a large freshwater lake. *Boundary-Layer Meteorology,* 148, 479-494. doi:10.1007/s10546-013-9827-9

Yang, K., et al., 2018. Spatial and temporal variations in the relationship between lake water surface temperatures and water quality - A case study of Dianchi Lake. *Science of the Total Environment,* 624, 859–871. doi: 10.1016/j.scitotenv.2017.12.119

Table 1. Previous studies on spatial variability of variables over lake surfaces

Reference	Lake, area and mean depth	Target variables Target area(s)	Method of measurements/estimation Spatial resolution Time resolution Target period	Method of variability analysis	Main findings*	Causes of variability	Homogeneity
Mahler and Assouline (1993)	Lake Kinneret, Israel (170 km^2, 2.6 m)	● Evaporation *E* ● East-west cross section (length of about 9.5 km) passing through the northern part of the Lake	● The two-dimensional mesoscale numerical model ● 1.5 km ● 45 s ● Daily means for 40 days during the September-October period	● Inspection of horizontal variation along the transect	● The daily *E* difference between the western shore, the eastern shore, and the center was as high as 50% of the largest *E* during the September-October period.	● Variability of wind speed and air-surface temperature difference	● Not studied
Lofgren and Zhu (2000)	Lake Huron, Canada/USA (59570 km^2, 53 m)	● **Energy balance** (latent L_eE and sensible heat flux *H*, net radiation (R_n), heat flux into a lake water body (*G*)) ● **Whole lake**	● The bulk method with surface temperature from remote sensing (NOAA AVHRR) and interpolated values of air temperature, humidity and wind speed measured at stations surrounding the Great Lakes ● 10 km grid ● Month ● 1992-1995	● Mapping monthly mean energy balance components ● Spatial mean and standard deviation of each month were tabulated.	● Considerable horizontal variation was found (standard deviation from 2-25 W/m^2 (L_eE), 2-58 W/m^2 (*H*), 3-13 W/m^2 (R_n), and 7-73 W/m^2 (*G*).	● The geographical difference of season progress	● Not studied

Anttila et al. (2008)	Lake Vesijärvi Finland (110 km^2; 6.8 m)	● Water quality (chlorophyll-a) ● Transects (average length of 20 km) in Enonselkä basin (26 km^2)	● Continuous water sampling along transects by a moving boat. ● 5-s interval along transects (corresponding approximately to 14 m) ● 4 surveys (4 days)	● Semivariogram analysis	● Point samples are only representative over a very limited area, due to the patchiness in chlorophyll a concentration.	● Not studied	● **Studied**
Alcântara et al. (2010)	Itumbiara reservoir (814 km^2, 21 m)	● Surface temperature T_s and heat flux into a lake water body ● **Whole lake**	● Bulk method (turbulent flux) with surface temperature from remote sensing (MODIS) and solar radiation, air temperature, humidity and wind speed measured at a single station ● 1 km ● daytime and nighttime monthly averages ● 786 daytime and 473 nighttime images in 2003-2008	● Mapping monthly mean surface temperature (nighttime and daytime) and heat flux into a water body	● Considerable horizontal variation of T_s (the range: 4.5-15°C (daytime) and 4-12.5°C (nighttime) ● T_s decreases (daytime) and increases (nighttime) from the shoreline to the center of the reservoir.	● The difference of water depth ● Advected heat with predominant wind direction	● Not studied
Sima et al. (2013)	Urmia Lake, Iran (2366 km^2, 5 † m)	● Surface temperature and evaporation *E* ● **Whole lake**	● Bowen ratio method using mean monthly surface temperature measured at a single location and monthly lake-	● Comparison of two sets of daytime monthly *E* estimate in 2009	● Annual *E* was determined to be 885 mm and 1,033 mm, respectively, suggesting significant variability in evaporation	● Variability of surface temperature	● Not studied

			averaged surface temperature using satellite remote sensing (MODIS) ● 1 km grid ● daytime and nighttime monthly averages ● 805 images in 2007-2010					
Wang et al. (2014)	Lake Taihu, China (2400 km^2, 1.9 m)	● **Energy balance** ● Footprint area of three sites	● Eddy correlation method and a radiometer at three sites located near the shoreline ● Size of a foot print area (not specified) ● 30 min ● 2011-2012	● Comparison of three sites	● On a diurnal time scale, considerable differences between sites existed but tended to vanish on longer time scales of seasons to years	● Water depth and wind speed differences	● Not studied	
Moukomala and Blanken (2017)	Great Lakes, Canada, and the USA (244783 km^2, 93 m)	● Evaporation *E* ● **Whole lake**	● Buk method with surface temperature from remote sensing (MODIS) and air temperature and wind speed from reanalysis data ● 1 km grid ● Month ● July 2001 to December 2014	● Mapping monthly lake evaporation	● Considerable horizontal variation of *E* was found (standard deviation from 0.1 to 2.3 mm/month)	● The movement of synoptic-scale air masses	● Not studied	

Woolway and Merchant (2018)	19 large lakes in the Northern Hemisphere	• Long term trend of surface temperature T_S • Stratification onset and stratified warming period • **Whole lake**, and the shallowest and deepest regions	• T_S data from the Along Track Scanning Radiometer (ATSR) Reprocessing for Climate: Lake Surface Water Temperature & Ice Cover (ARC-Lake) product • 0.05° grid • daily • 1991-2011 (variable length depending on lakes)	• Linear trend analysis • Comparison of stratification onset and stratified warming period between the shallowest and deepest regions	• Later onset of thermal stratification, shorter stratified warming period, and the longer time scale over which variations in stratification onset have a significant influence on T_S anomalies in the deepest areas than in the shallowest areas • Higher rates of warming of summer T_S in the deepest areas than in the shallowest areas	• Deep convective mixing in the deepest regions having larger thermal inertia than in the shallowest regions.	• Not studied
Rahaghi et al. (2019)	Lake Geneva (582 km^2, 152.7 † m)	• Surface temperature T_S and surface cooling rate (outgoing long-wave radiation, and sensible and latent heat fluxes) • The northern part of the lake	• Buk method (turbulent flux) and Stefan-Boltzmann equation (radiation) • The thermal infrared imager on a tethered balloon and in situ measurements of near-surface water and air properties, • 0.8-2.7 m resolution in 1.4 ×1.4 km area (offshore) • Four daytime missions under calm-	• Comparison of maps of T_S, cooling rate and atmospheric stability	• The considerable variation of T_S and cooling rate was observed. • T_S variation of a horizontal scale of 1-10 m was dominant.	• T_S and atmospheric stability (for cooling rate) • Atmospheric stability. Also, the influence of net surface energy, surface mixing, and water stratification were suggested (for surface temperature)	• Not studied

			wind condition in 2016-17.					
This study	Lake Kasumigaura (Nishiura), Japan (172 km^2, 4 m)	• **Energy balance** (latent and sensible heat flux, net radiation, heat flux into a lake water body • **Whole lake**	• The bulk method with surface temperature from remote sensing (ASTER) and interpolated values of air temperature, humidity and wind speed measured at stations in and surrounding Lake Kasumigaura) • **90 m grid** • Snapshot • Three clear-sky cases under different wind conditions	• Mapping energy balance components • Inspection of horizontal variation along the transects • Semivariogram analysis of T_s	• Spatial variations are apparent for energy balance components except for net radiation • Two horizontal scales (10^3-10^4 m, and 10^2) of variations exist. • Distinctive fluxes were found near the shorelines • Surface temperature is homogeneous only in the central part of Lake Kasumigaura which can be judged suitable for flux measurements	• Spatial variations of air temperature, humidity and wind speed at the regional scale (for flux variation of 10^3-10^4 m scale) • Spatial surface temperature variation of the scale of 10^2 m (for small scale flux variation) • Shallow depth and presence of reed communities and breakwaters near the shorelines (for distinctive fluxes	• **Studied**

					near the shorelines)

Those items relevant for the present study are indicated by bold face.

* those related to the present study purposes.

† from World Lake Database (ILCF 2019).

Table 2. Meteorological conditions and some of the results over Lake Kasumigaura for the three cases.

Case	Date	U (m/s)	Wind direction	T_s (°C)	T_a (°C)	q (kg/kg)	z/L	H (W/m^2)	L_eE (W/m^2)	R_n (W/m^2)	G (W/m^2)
I	21 Nov. 2007	2.76±0.63	NE to N	13.5±0.6	9.9±0.2	0.00378±0.00012	-0.15	21.2±5.4	24.7±9.7	421.9±3.3	376.7±15.7
		0.23		0.05	0.02	0.03		0.25	0.39	0.01	0.04
		-0.80		0.09	0.77	-0.39		2.06	0.64	-0.16	-0.19
		-0.26		4.74	0.01	-0.79		14.79	3.19	4.91	2.62
II	7 Dec. 2007	0.85±0.11	Variable	11.3±0.7	9.9±0.3	0.00561±0.00050	-8.2	7.4±4.7	20.4±5.9	361.9±3.6	334.0±13.0
		0.13		0.06	0.03	0.09		0.64	0.29	0.01	0.04
		0.51		3.19	0.38	-0.41		3.38	2.44	-3.29	-3.13
		0.91		17.56	0.23	-0.75		21.04	13.54	18.40	18.14
III	1 Jan. 2009	7.19±1.68	NW to W	6.8±0.7	6.2±0.2	0.00249±0.00008	-0.02	4.3±5.4	81.9±19.1	383.8±3.5	297.5±25.2
		0.23		0.10	0.03	0.03		1.25	0.23	0.01	0.08
		1.11		2.85	1.08	0.74		2.41	0.61	-2.97	-1.05
		0.05		17.46	0.50	1.48		14.03	4.17	18.30	5.07

z/L was determined from the mean fluxes of H and L_eE and friction velocity values measured at the Koshin observatory. In other columns, the 1st raw indicates the mean ± standard deviation; 2nd raw gives the coefficient of variation (CV), 3rd raw lists skewness, and 4th raw the kurtosis.

Table 3. Temperature, wave, and lake current at the Koshin observatory for the three cases.

	Case I	Case II	Case III
Date	21 Nov. 2007	7 Dec. 2007	1 Jan. 2009
T_s	14.3	12.5	9.1
T_w at −1 m	14.0	10.8	7.2
T_w at −2.5 m	13.7	10.3	7.0
Significant wave height (m)	0.15	0.07	0.41
Significant wave period (s)	1.53	1.34	2.28
Lake current at −0.75 m (m/s)	0.025	0.018	0.040*

T_w: water temperature; *: estimated from wind speed at Koshin Observatory and empirical equation between Lake currents and wind speeds obtained from Wei et al. (2016)

Table 4. Results of the semivariogram assessment of surface temperature, T_s.

Angle ± Tolerance (°)	Range (m)		
	Case I	Case II	Case III
0±30	NH	4000, 9000**	NH
30±30	NH	4000*, **	NH
60±30	8000*, **	4000*, **	8000**
90±30	5000*, **	4000*, **	NH
120±30	7000**	4000**	NH
150±30	NH	7000**	2000**
0±90	NH	3500**	NH

Angle is defined in a standard mathematical convention, and 0° is toward the east (positive *x*-direction) and 90° is toward the north (positive *y*-direction). NH: Range does not exist (nonhomogeneous). *: the presence of hole(s). **: nested structure.

Figure caption

Figure 1. A map of the study area. Depth contour lines with a 0.5-m interval are shown within Lake Kasumigaura (Nishiura). Three cross-sectional lines are also indicated (a horizontal variation of variables along the lines is shown in Fig. 3). Circular subregions in Tsuchiura-iri and in Koshin are also indicated (see Section 4.2). Circles denote meteorological stations (see Sugita et al., 2014 for details).

Figure 2. The spatial distribution of (a) R_n, (b) G, (c) L_eE, (d) H, (e) $(q_s - q)$, (f) $(T_s - T)$, (g) U, (h) C_H, (i) q, (j) T, and (k) T_s scaled by equation (11) for Case I.

Wind speed and wind direction measured at the stations are also shown as arrows in (g). The geographical center determined by equation (12) is indicated by a cross and the weighted geographical center in equation (13) by a closed circle.

Figure 3. The horizontal variation of T_s, $(T_s - T)$, H, U, and C_H scaled by equation (11) and of the depth along the three cross-sectional lines (A-A', B-B', and C-C') shown in Fig. 1 in Lake Kasumigaura for Case III.

Figure 4. A semivariogram of T_s normalized by the spatial variance of T_s over Lake Kasumigaura for Case I. Both the directional and omnidirectional semivariograms are shown. The directional semivariogram is given for six directions $\pm 30°$; the zero direction indicates the North-South direction and 90° is the East-West direction. The omnidirectional semivariogram is given for $0° \pm 90°$ (i.e., in all directions).

Figure S1. The spatial distribution of (a) R_n, (b) G, (c) L_eE, (d) H, (e) $(q_s - q)$, (f) $(T_s - T)$, (g) U, (h) C_H, (i) q, (j) T, and (k) T_s scaled by equation (11) for Case II.

Wind speed and wind direction measured at the stations are also shown as arrows in (g). The cross and closed circle in each panel represents the geographical center, z_1, and the centroid, z_2, respectively.

Figure S2. The same as Fig. S1 but for Case III.

Figure S3. The lake current observed at 15:40 on 31 December 2007 (INA Corporation, 2008) under a northwesterly wind, a similar condition to Case III.

Solid arrows represent the direction and magnitude of (a) wind speeds at 10 m, (b) lake current velocities at −0.25 m, (c) those at −2.25 m, and (d) those at −3.75 m. Dotted arrows indicate estimated flow directions based on the analysis of extensive measurements by the INA Corporation.

Figure S4. Semivariogram of T_s over Lake Kasumigaura for Case II. Both the directional and omnidirectional semivariograms are shown. The directional semivariogram is given for six directions ±30°; the zero direction indicates the North-South direction and 90° indicates the East-West direction. The omnidirectional semivariogram is given for 0° ±90° (i.e., all directions).

Figure S5. The same as Fig. S4 but for Case III.

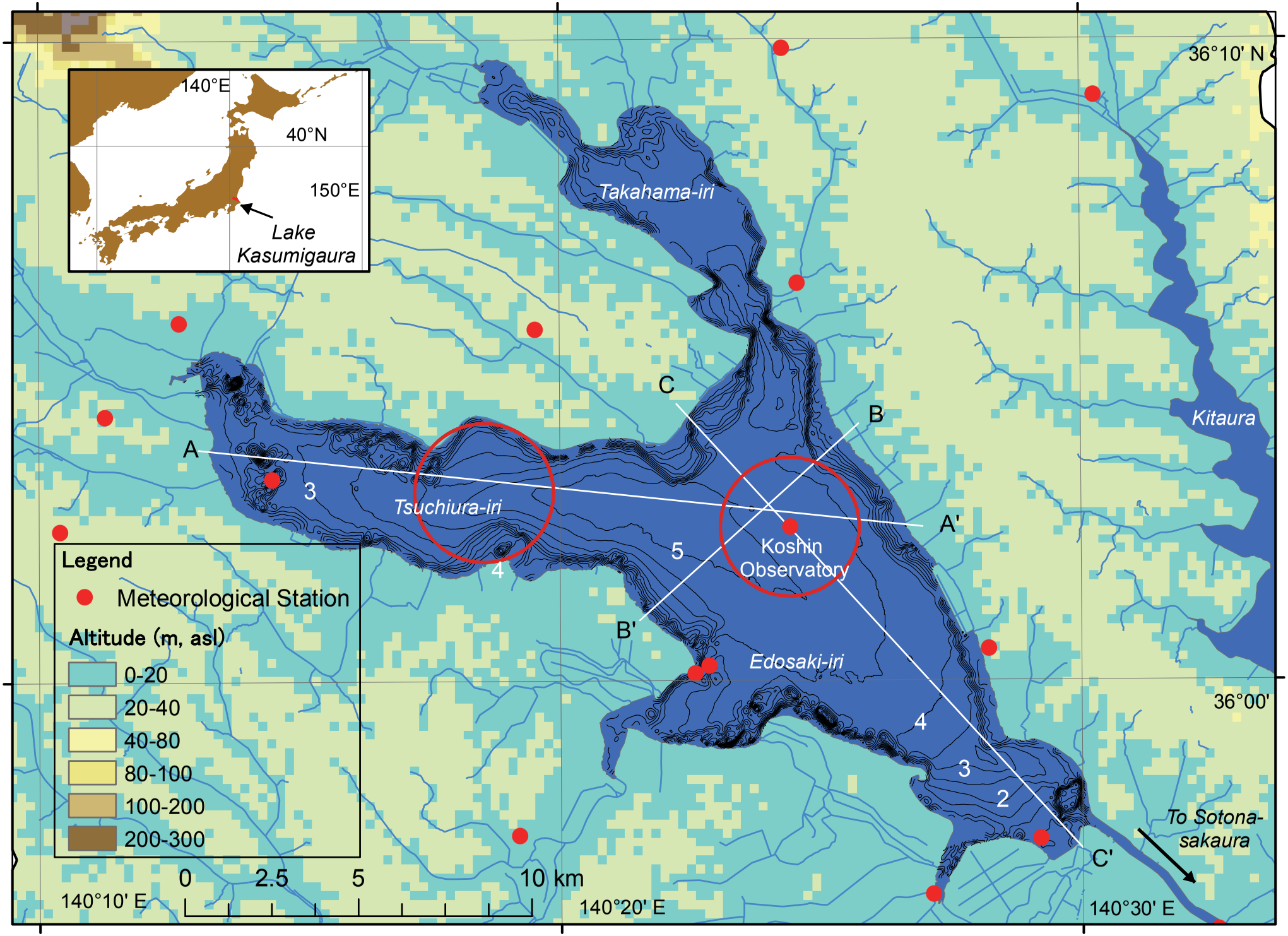
140°E
40°N
150°E
Lake Kasumigaura
Takahama-iri
Kitaura
Tsuchiura-iri
Koshin Observatory
Edosaki-iri
A
A'
B
B'
C
C'
3
4
5
4
3
2
To Sotona-sakaura
Legend
Meteorological Station
Altitude (m, asl)
0-20
20-40
40-80
80-100
100-200
200-300
0
2.5
5
10 km
36°10' N
36°00'
140°10' E
140°20' E
140°30' E

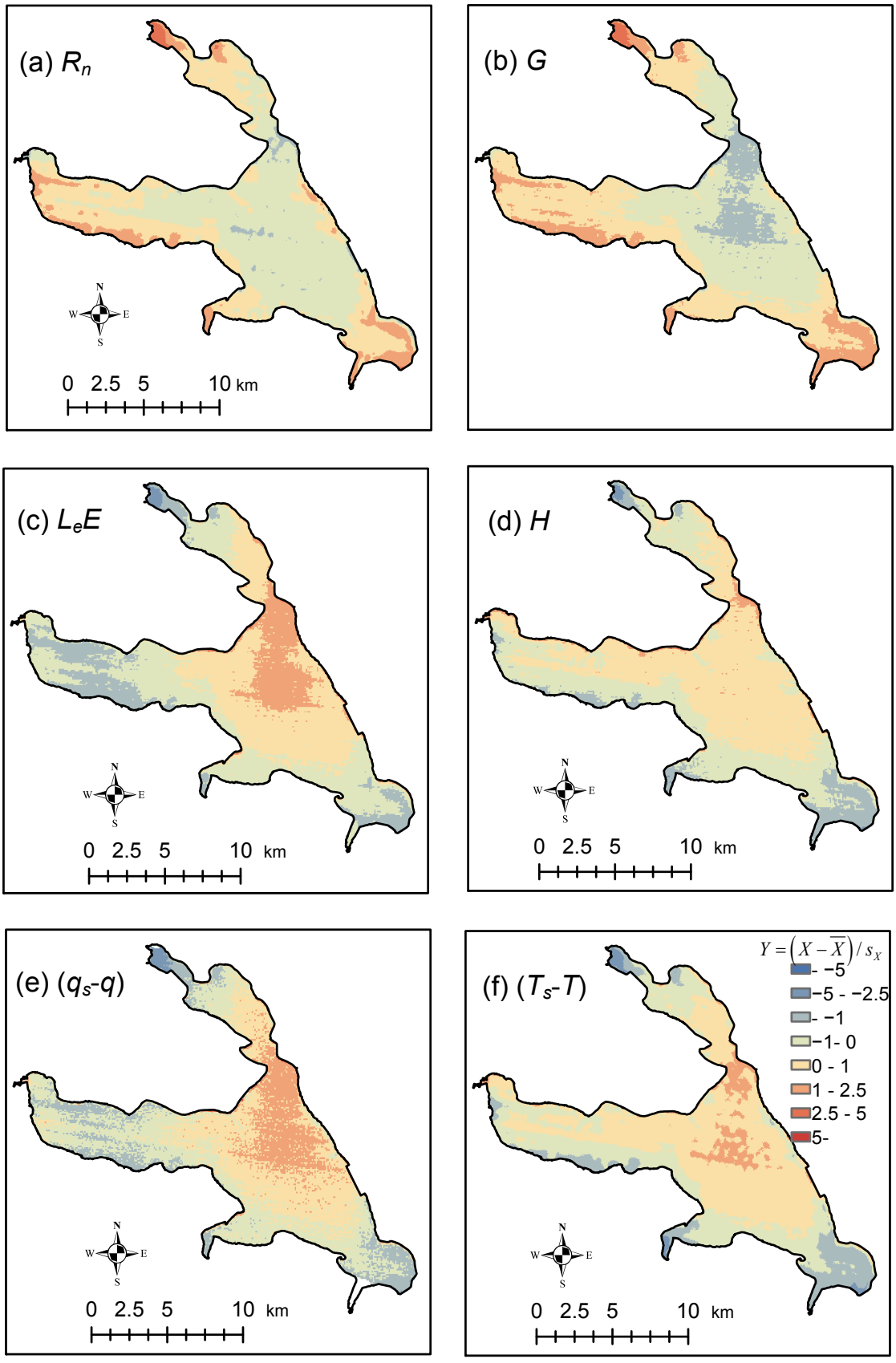
(a) R_n
(b) G
(c) L_eE
(d) H
(e) (q_s-q)
(f) (T_s-T)
N
W
E
S
0 2.5 5 10 km
$Y = (X - \overline{X}) / s_X$
- −5
−5 - −2.5
- −1
−1- 0
0 - 1
1 - 2.5
2.5 - 5
5-

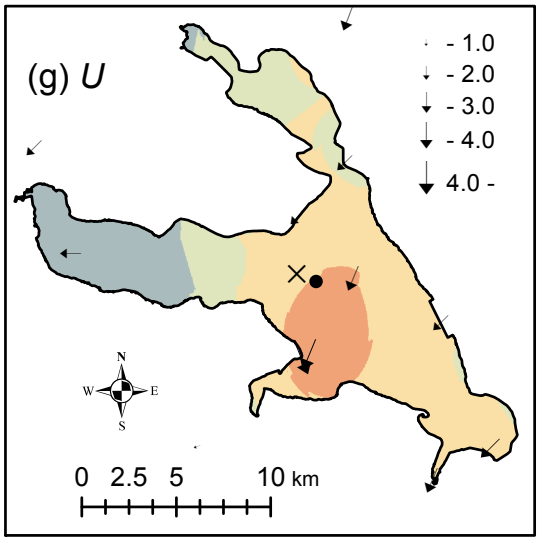

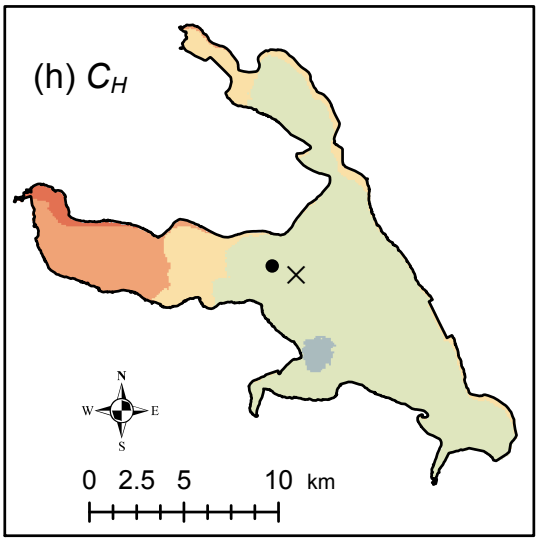

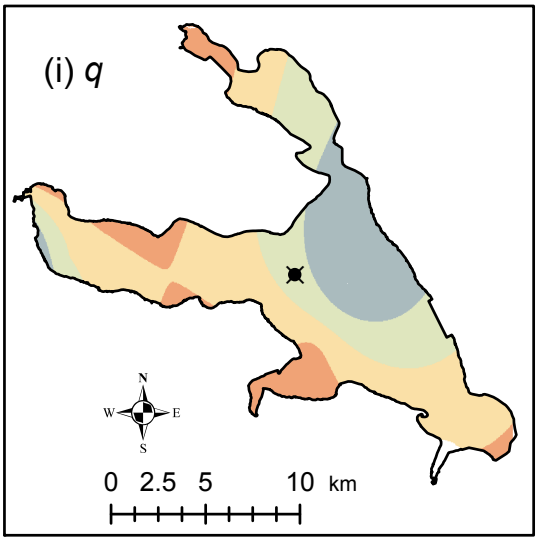

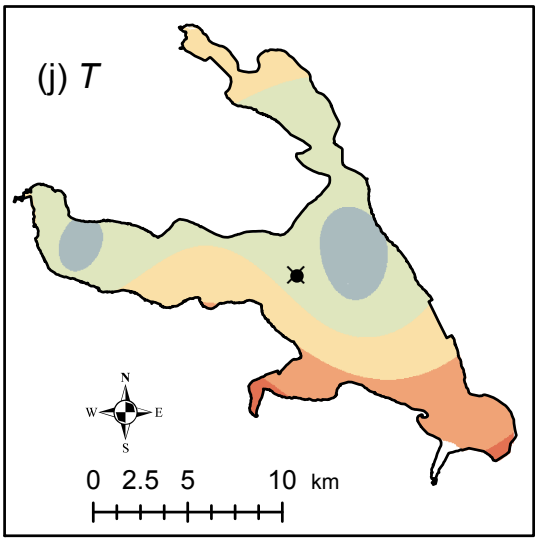

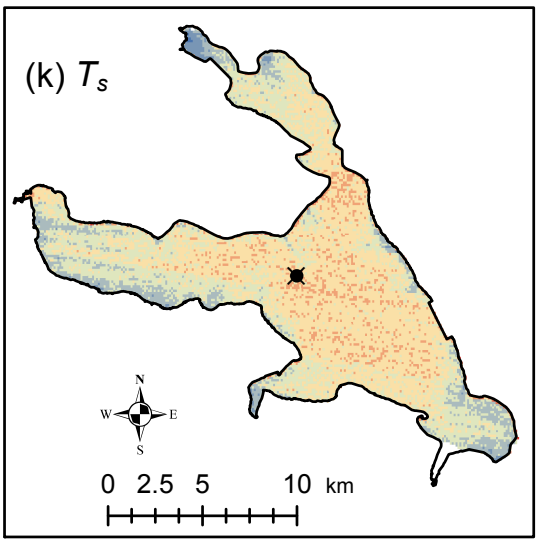

$Y = \left(X - \overline{X}\right) / s_X$

- −5
−5 - −2.5
- −1
−1- 0
0 - 1
1 - 2.5
2.5 - 5
5-

× Geographical center by eq. (12)

● Weighted geographical center by eq.(13)

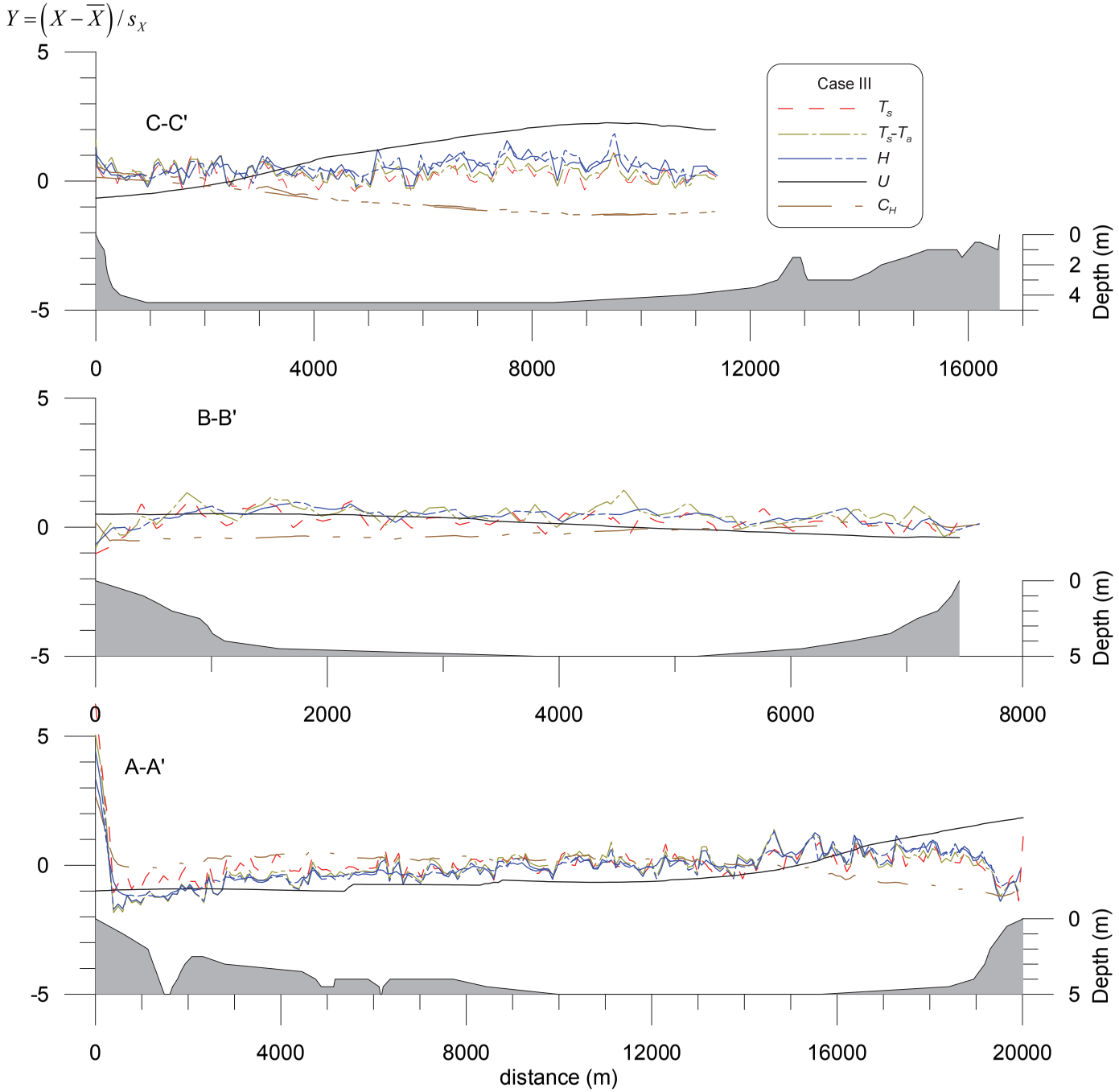
$Y = \left(X - \overline{X}\right) / s_X$
C-C'
B-B'
A-A'
Case III
T_s
T_s-T_a
H
U
C_H
5
0
-5
0
4000
8000
12000
16000
2000
6000
20000
2
4
Depth (m)
5
distance (m)

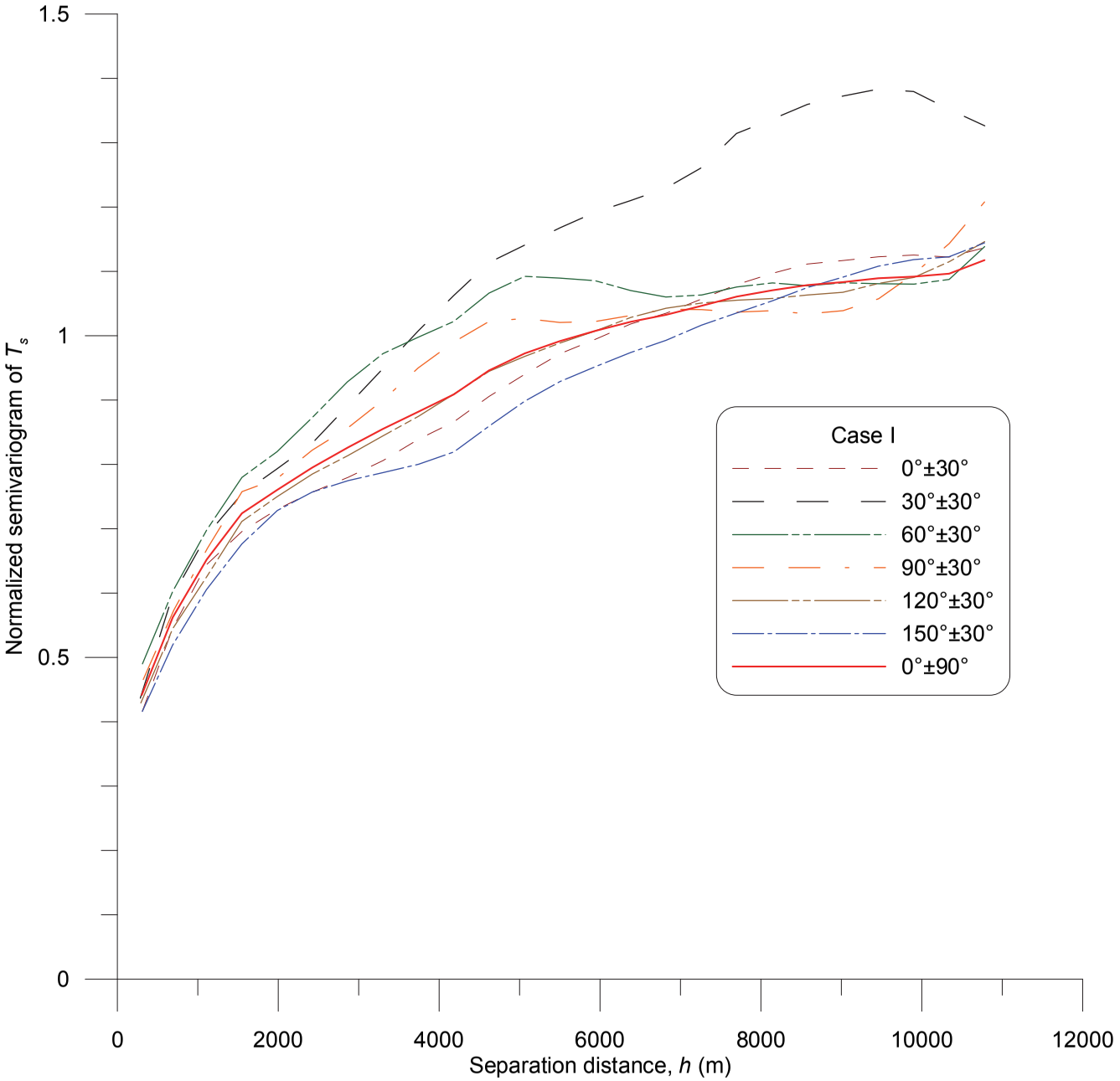
1.5
1
0.5
0
Normalized semivariogram of T_s
0
2000
4000
6000
8000
10000
12000
Separation distance, h (m)
Case I
0°±30°
30°±30°
60°±30°
90°±30°
120°±30°
150°±30°
0°±90°

Spatial Variability of the Surface Energy Balance of Lake Kasumigaura and Implications for Flux Measurements

by Michiaki Sugita

Supplementary material

1. Method to determine Equation (6)

The ratio of C_H/C_{HN}:

$$\frac{C_H}{C_{HN}} = \frac{C_E}{C_{EN}} = \left[1 - \Psi_H(\zeta)/\ln(z/z_{0h})\right]^{-1}\left[1 - \Psi_M(\zeta)/\ln(z/z_0)\right]^{-1} \qquad (6)$$

was determined for each of the three cases, as follows.

First, $\zeta = z/L$ was estimated from the bulk Richardson number, Ri_B, defined as:

$$Ri_B = -\frac{gz(T_s - T)}{T_a U^2} \qquad (S.1)$$

where T_a is equal to T but in Kelvin. Ri_B can be determined at each pixel from available data and interpolated values. Although Ri_B is related to ζ by:

$$\zeta = Ri_B \frac{\left(\ln(z/z_0) - \Psi_M(\zeta)\right)}{\left(\ln(z/z_{0h}) - \Psi_H(\zeta)\right)}, \qquad (S.2)$$

Eq. (S.1) is implicit and it is not straightforward for directly determining ζ from Ri_B. Thus, an empirical equation $\zeta = f(Ri_B)$ was derived for each of the three cases by fitting a curve to the pair of values of ζ and Ri_B. Three pair of values for the three cases were obtained by calculating Ri_B from ζ using inverted Eq. (S.2), with values of z_{0h} and z_0 determined at the Koshin observatory.

Once ζ has been determined, Eq. (6) was calculated based on the values of Ψ estimated by means of integrated forms of the Businger-Dyer relationship (e.g., Brutsaert 1982).

Spatial Variability of the Surface Energy Balance of Lake Kasumigaura and Implications for Flux Measurements: Supplementary materials by M.Sugita

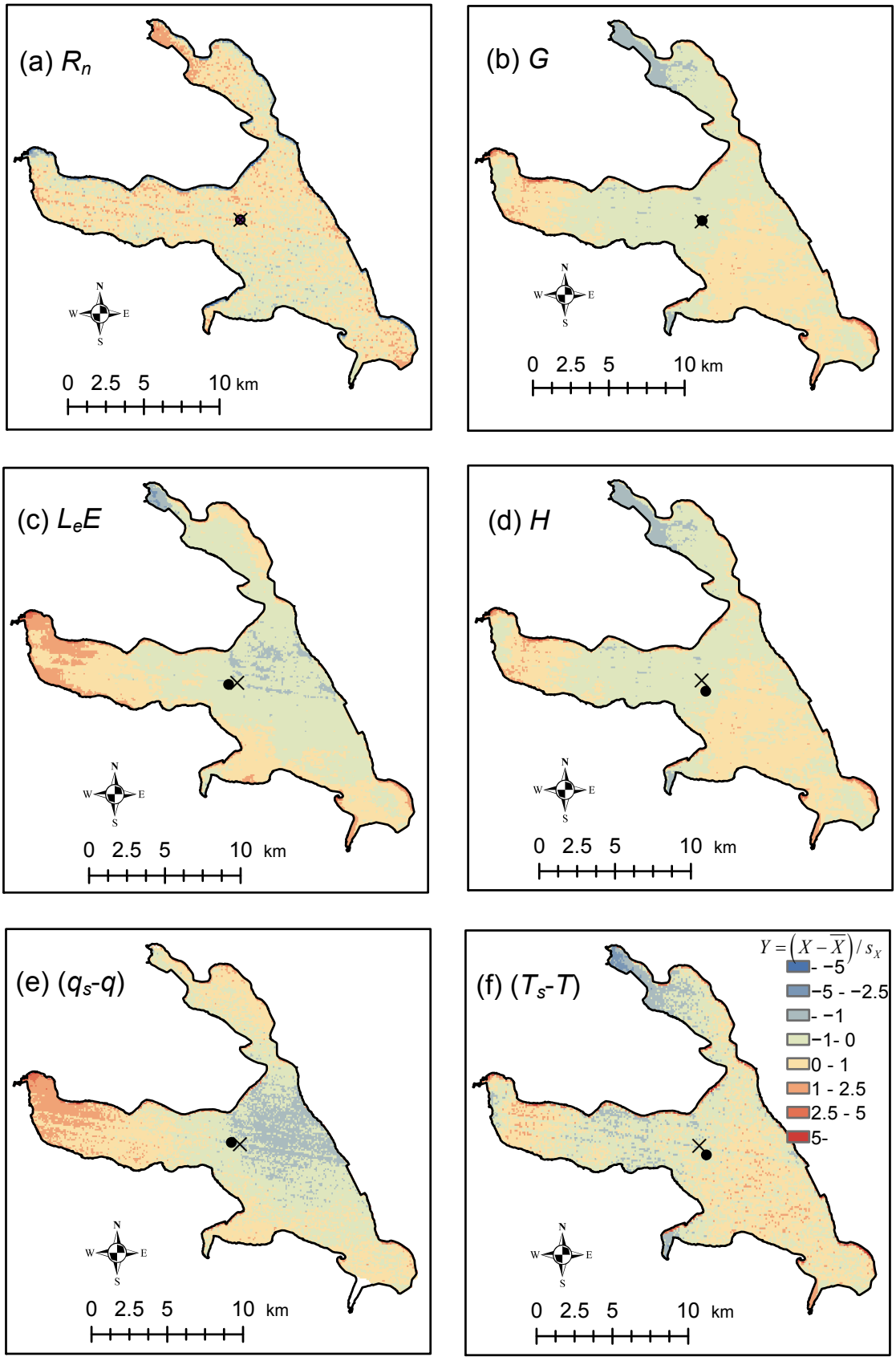

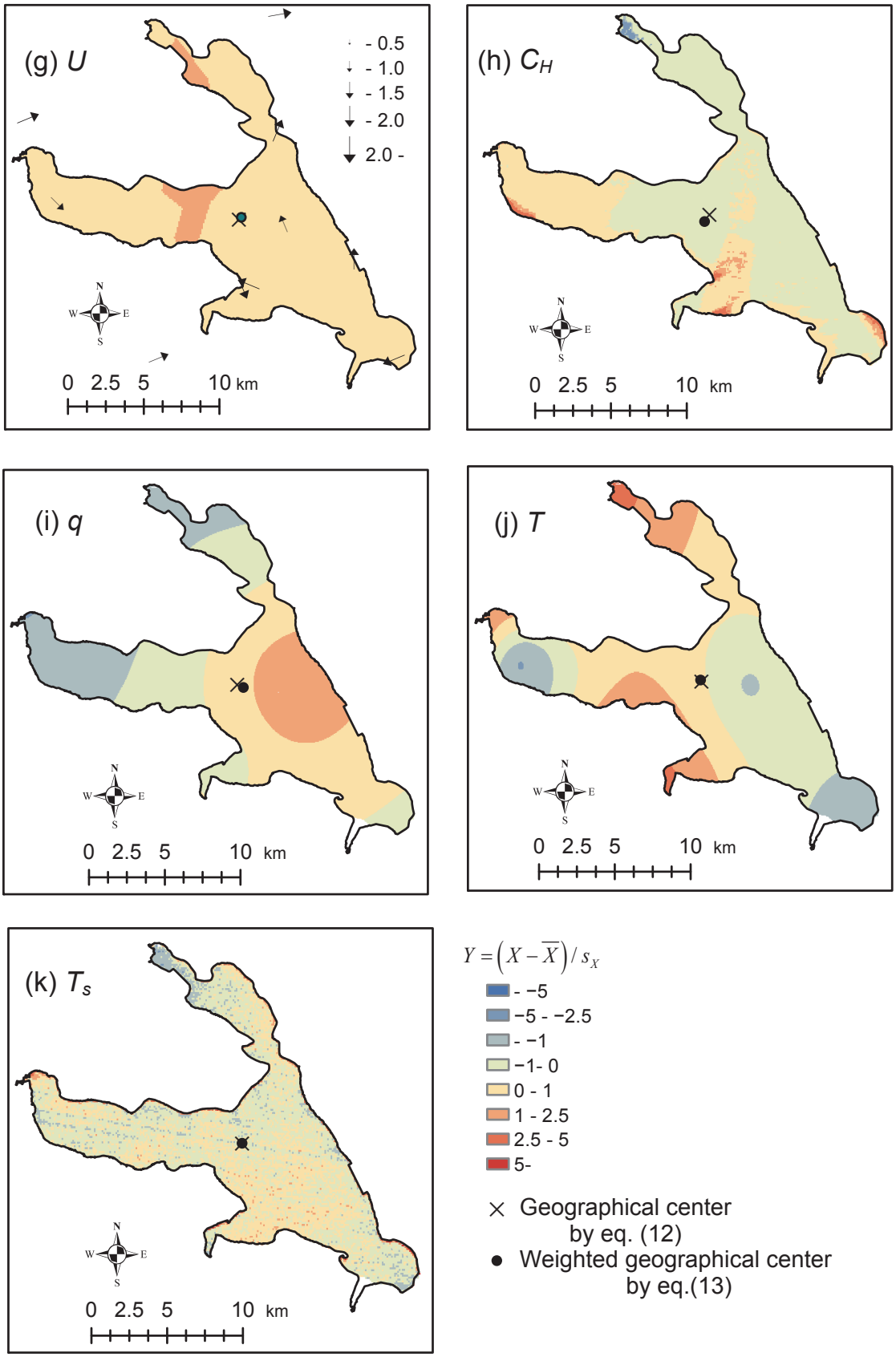

Figure S1. The spatial distribution of (a) R_n, (b) G, (c) L_eE, (d) H, (e) , (f) , (g) U, (h) C_H, (i) q, (j) T, and (k) T_s scaled by equation for Case II. Wind speed and wind direction measured at the stations are also shown as arrows in (g). The cross and closed circle in each panel represents the geographical center, z_1, and the centroid, z_2, respectively.

Spatial Variability of the Surface Energy Balance of Lake Kasumigaura and Implications for Flux Measurements: Supplementary materials by M.Sugita

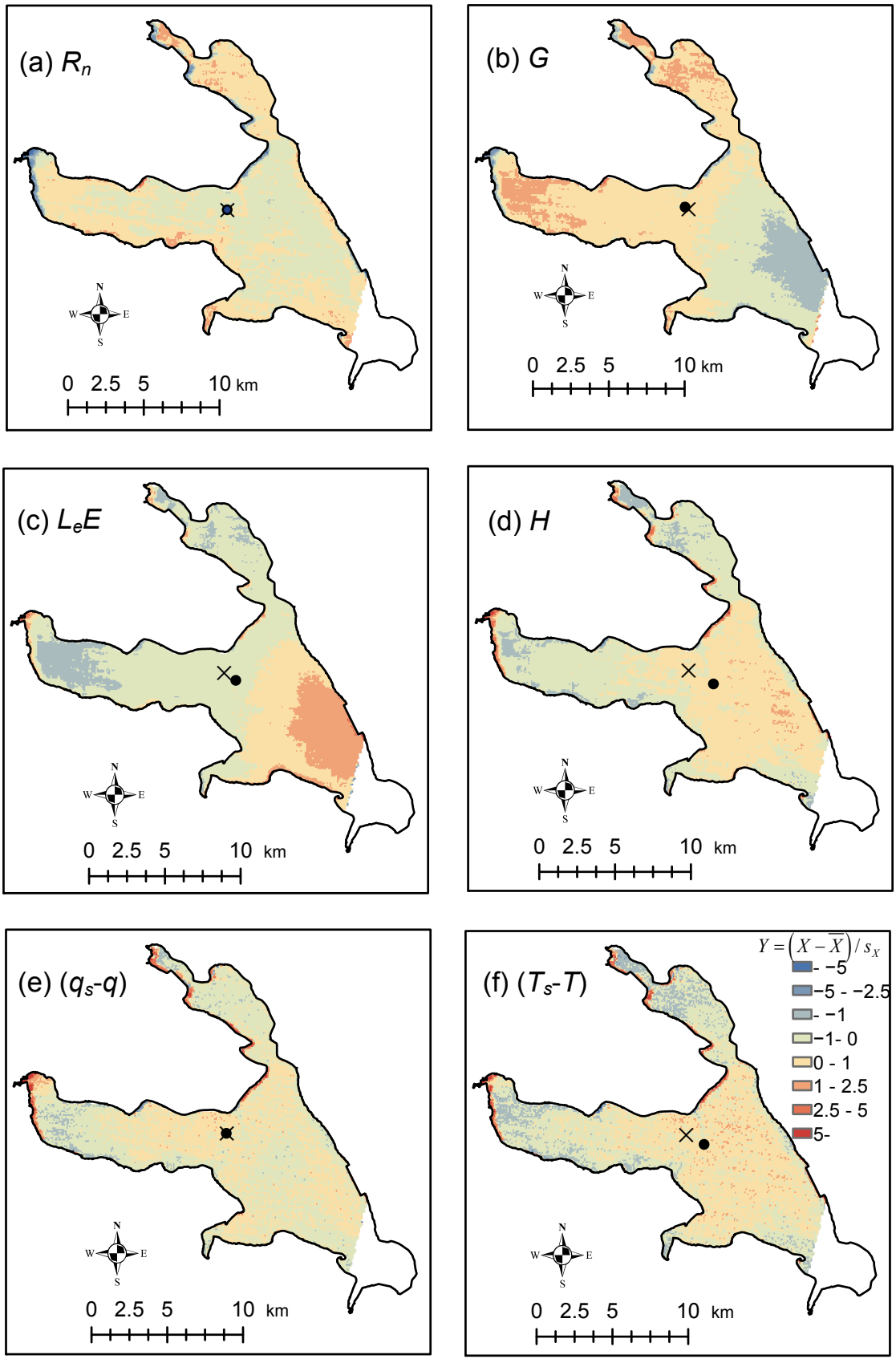

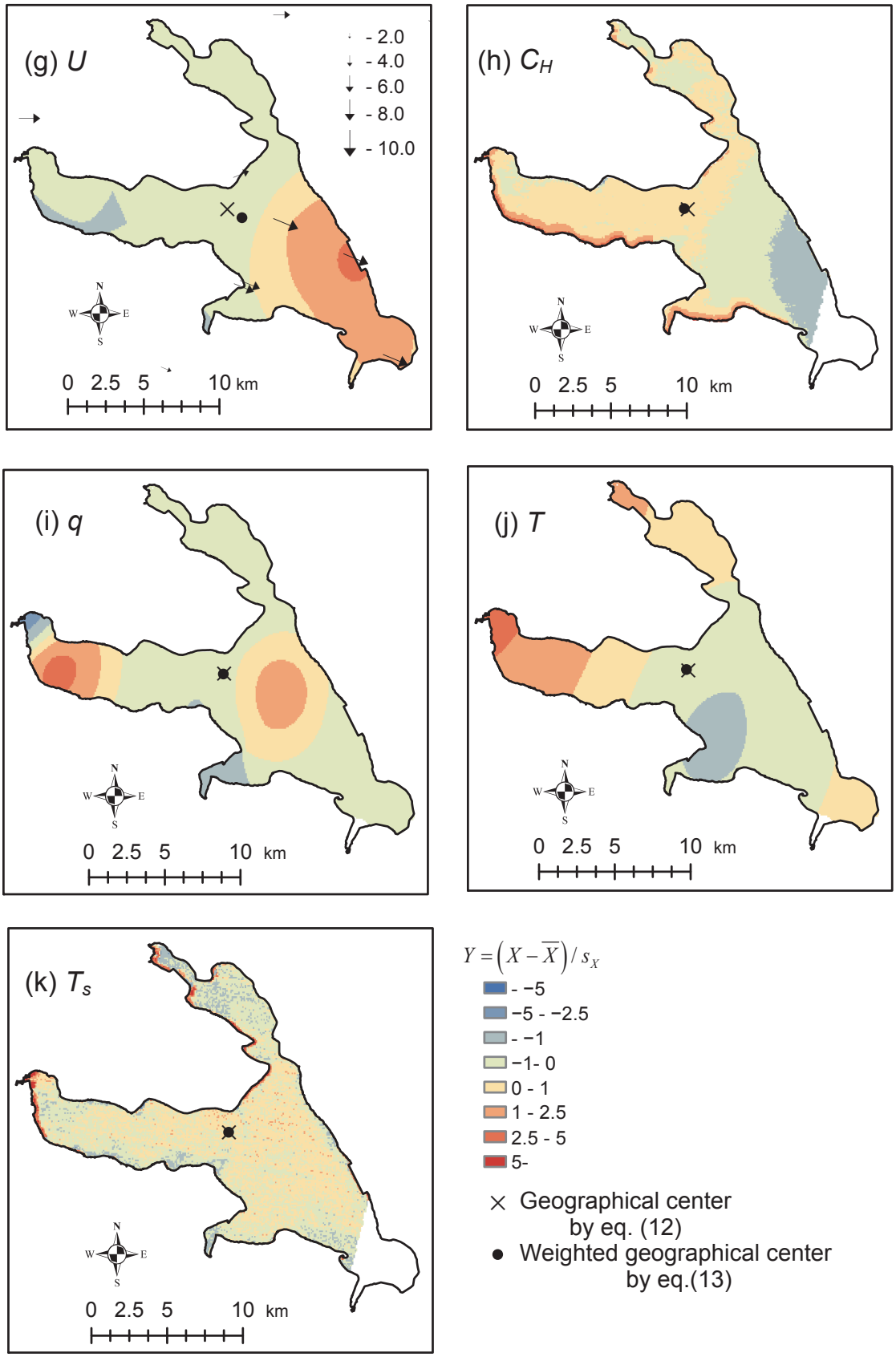

Figure S2. The same as for Fig. S1 but for Case III.

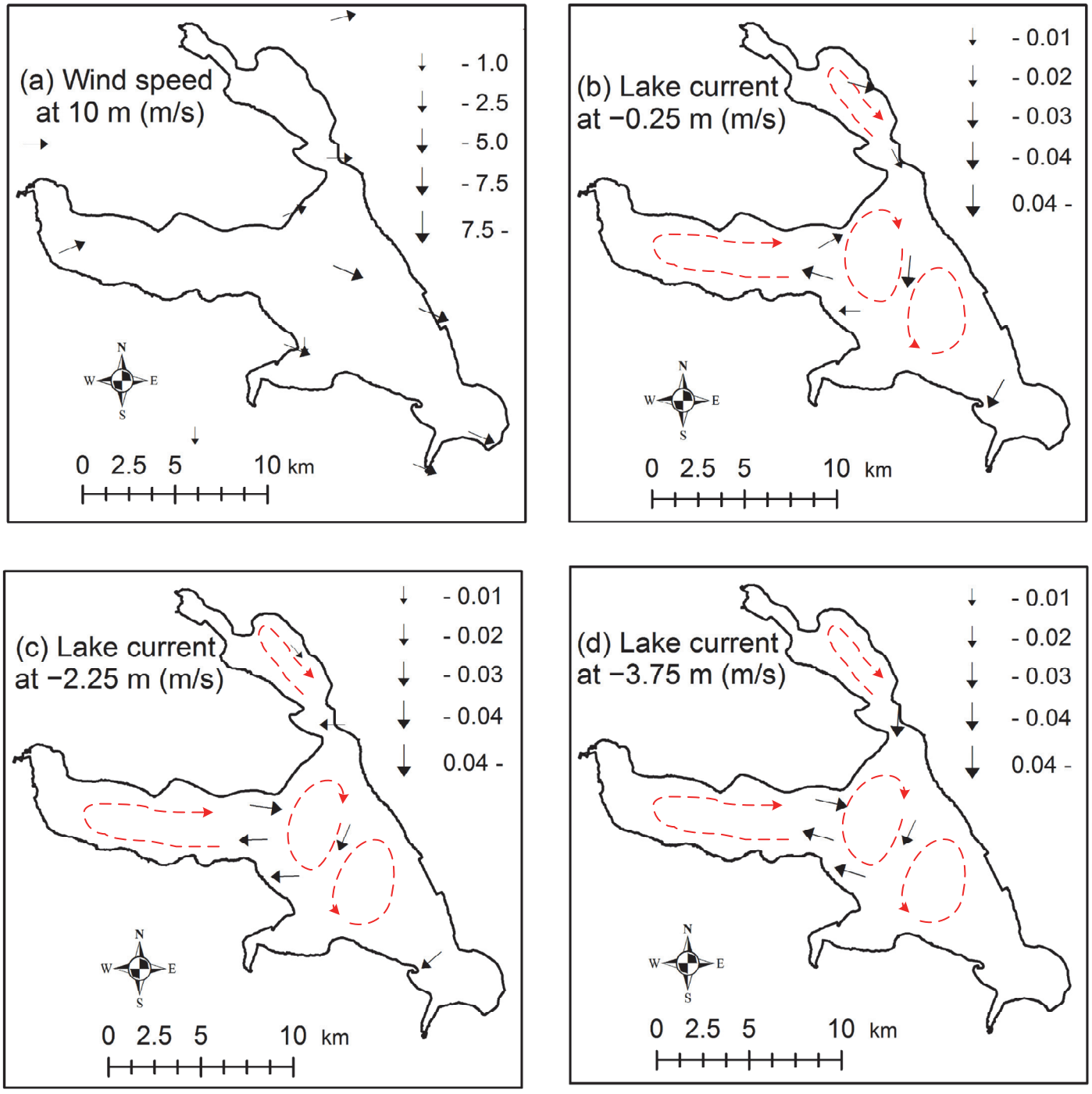

Figure S3. Lake current observed at 15:40 on December 31, 2007 (INA Corporation, 2008) under the northwesterly wind, a similar condition to Case III. The solid arrows represents direction and magnitude of (a) wind speeds at 10 m, (b) lake current velocities for at −0.25 m, (c) velocities at −2.25 m, and (d) velocities at −3.75 m. Dotted arrows indicate estimated flow direction based on the measurements and analysis of extensive measurements by INA Corporation.

Spatial Variability of the Surface Energy Balance of Lake Kasumigaura and Implications for Flux Measurements: Supplementary materials by M.Sugita

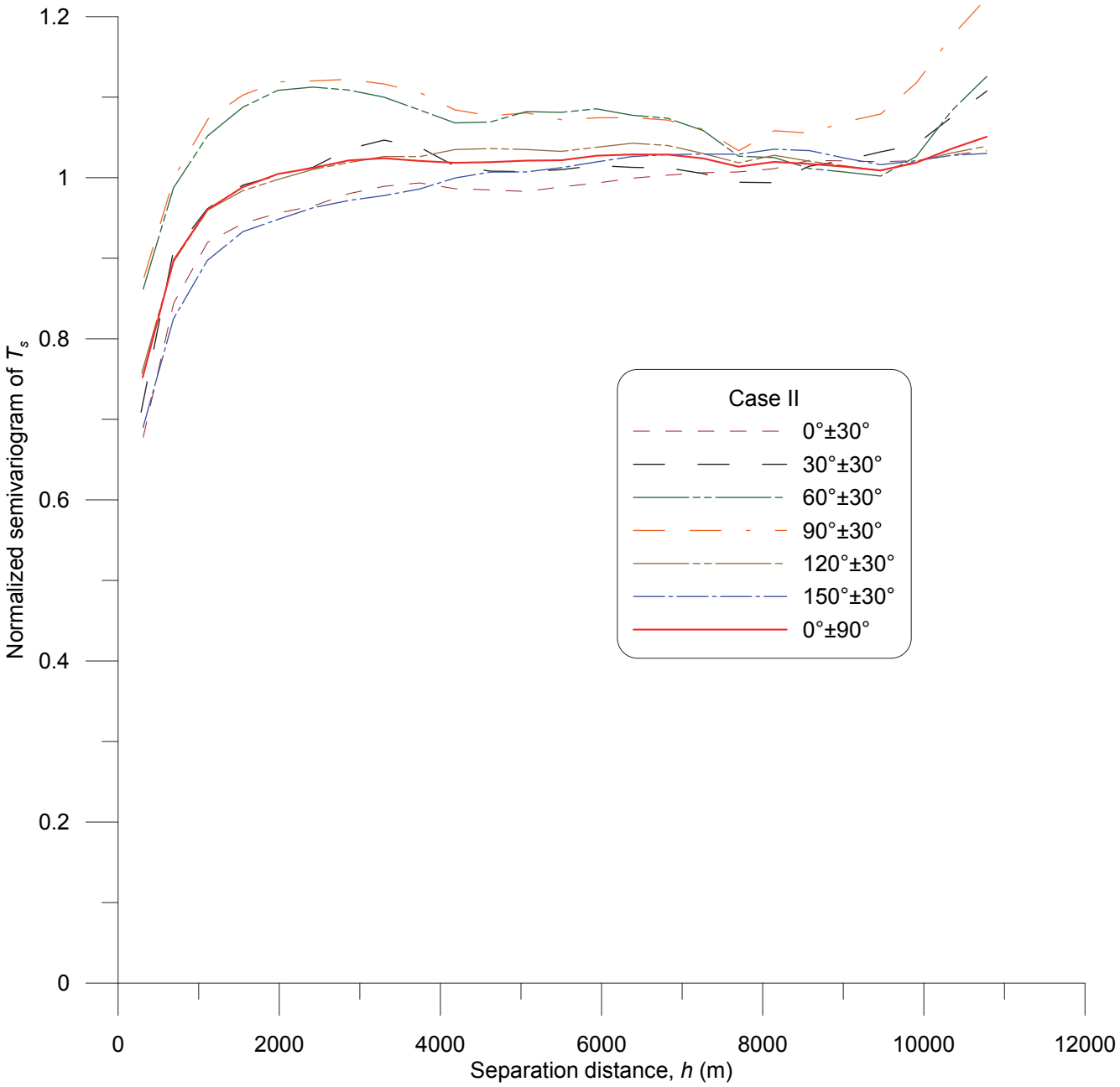

Figure S4. Semivariogram of T_s normalized by the total spatial variance of T_s over Lake Kasumigaura for Case II. Both the directional and omnidirectional semivariograms are shown. The directional semivariogram is given for six directions ±30°; the zero direction indicates the North-South direction and 90° indicates the East-West direction. The omnidirectional semivariogram is given for 0°±90° (i.e., all directions).

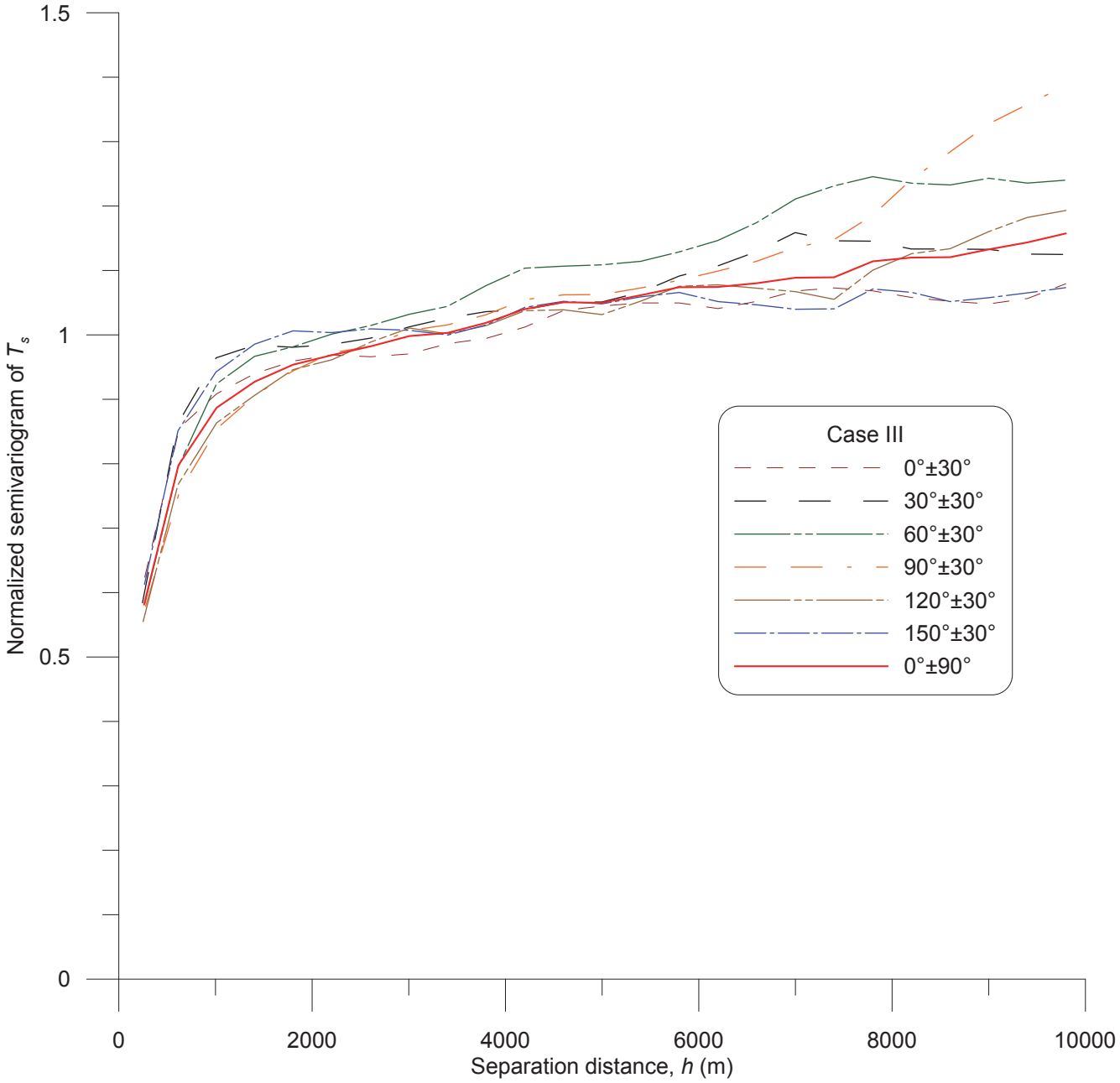

Figure S5. The same as for Fig. S4 but for Case III.